

ADVERTIMENT. La consulta d'aquesta tesi queda condicionada a l'acceptació de les següents condicions d'ús: La difusió d'aquesta tesi per mitjà del servei TDX (www.tesisenxarxa.net) ha estat autoritzada pels titulars dels drets de propietat intel·lectual únicament per a usos privats emmarcats en activitats d'investigació i docència. No s'autoritza la seva reproducció amb finalitats de lucre ni la seva difusió i posada a disposició des d'un lloc aliè al servei TDX. No s'autoritza la presentació del seu contingut en una finestra o marc aliè a TDX (framing). Aquesta reserva de drets afecta tant al resum de presentació de la tesi com als seus continguts. En la utilització o cita de parts de la tesi és obligat indicar el nom de la persona autora.

ADVERTENCIA. La consulta de esta tesis queda condicionada a la aceptación de las siguientes condiciones de uso: La difusión de esta tesis por medio del servicio TDR (www.tesisenred.net) ha sido autorizada por los titulares de los derechos de propiedad intelectual únicamente para usos privados enmarcados en actividades de investigación y docencia. No se autoriza su reproducción con finalidades de lucro ni su difusión y puesta a disposición desde un sitio ajeno al servicio TDR. No se autoriza la presentación de su contenido en una ventana o marco ajeno a TDR (framing). Esta reserva de derechos afecta tanto al resumen de presentación de la tesis como a sus contenidos. En la utilización o cita de partes de la tesis es obligado indicar el nombre de la persona autora.

WARNING. On having consulted this thesis you're accepting the following use conditions: Spreading this thesis by the TDX (www.tesisenxarxa.net) service has been authorized by the titular of the intellectual property rights only for private uses placed in investigation and teaching activities. Reproduction with lucrative aims is not authorized neither its spreading and availability from a site foreign to the TDX service. Introducing its content in a window or frame foreign to the TDX service is not authorized (framing). This rights affect to the presentation summary of the thesis as well as to its contents. In the using or citation of parts of the thesis it's obliged to indicate the name of the author

Universitat Politècnica de Catalunya

ICFO - The Institute of Photonic Sciences

Whispering Gallery Microresonator for Second Harmonic Light Generation

Jorge Luis Dominguez Juarez

Director: Professor Jordi Martorell

April 23rd, 2014

WHISPERING GALLERY MICRORESONATOR FOR
SECOND HARMONIC LIGHT GENERATION

JORGE LUIS DOMINGUEZ JUAREZ

Under de supervision of

PROFESSOR JORDI MARTORELL

submitted this thesis in partial fulfillment
of the requirements for the degree of

DOCTOR

By the

UNIVERSITAT POLITECNICA DE CATALUNYA

BARCELONA, 2014.

Acknowledgements

First to all, I thank to my academic advisor Jordi Martorell for giving me the opportunity to work in his lab, for the support and guidance at the final stage of my studies, for all that time I am heavily in debt. I would like to acknowledge Gregory for his important contribution in the progress of this thesis, I am really grateful for the enormous help. I would like also to thank Martorell's lab for helping me and support me all the time. Many thanks to the Institute of Photonic Sciences and the Universitat Politecnica de Catalunya for giving me the possibility to reach my academic dream. I am equally grateful to CONACYT for the five years of financial support. I also have to thank my family, friends and external people that supported me in this thesis.

Publications

J. L. Domínguez-Juárez, G. Kozyreff, J. Martorell. “Whispering gallery microresonators for second harmonic light generation from a low number of small molecules”. *Nature Commun.* 2, 254 (2011).

G. Kozyreff, **J. L. Domínguez-Juarez**, J. Martorell, “Nonlinear optics in spheres: from second harmonic scattering to quasi-phase matched generation in whispering gallery modes”. *Laser Photonics Rev.* 5, 737-749 (2011).

G. Kozyreff, **J. L. Domínguez Juárez**, J. Martorell. “Whispering-gallery-mode phase matching for surface second-order nonlinear optical processes in spherical microresonators”. *Phys. Rev. A* 77, 043817 (2008).

J. L. Domínguez-Juárez, R. Macovez, M. Ujue González, J. Martorell. “Molecular quadratic nonlinear susceptibility gratings via electron-beam lithography“. *Appl. Phys. Lett.* 97, 023307 (2010).

N. Lou, R. Jha, **J. L. Domínguez-Juárez**, V. Finazzi, J. Villatoro, G. Badenes, V. Pruneri. “Embedded optical micro/nano-fibers for stable devices”. *Opt. Lett.* 35, 571-573 (2010).

J. Bravo-Abad, X. Vidal, **J. L. Domínguez Juárez**, J. Martorell. “Optical second-harmonic scattering from a non-diffusive random distribution of nonlinear domains”. *Opt. Express* 18, 14202-14211 (2010).

F. J. Rodríguez, C. Yao, **J. L. Domínguez-Juárez**, J. Bravo-Abad, J. Martorell. “Observation of speckle pattern formation in transparent nonlinear random media”. *Opt. Lett.* 36, 1347-1349 (2011).

Contents

Publications.....	i
Abstract	1
Resumen.....	3
Resum	6
1. Introduction.....	8
Circular Optical Microresonators as Sensors.....	8
Nonlinear Optics in Circular Microresonators.....	10
Objectives and Outline	13
2. Whispering Gallery Modes and Surface SHG.....	15
Introduction.....	15
Circular Optical Microresonators	15
Fused Silica Spherical Microresonators	18
Coupling Light in a Microsphere.....	19
Understanding the WGM Propagation of Light Inside a Micro-Sphere.....	21
Surface SHG in Whispering Gallery Modes	25
Phase Matching and Coherence Length.....	26
Quasi-Phase Matching for SHG using WGM.....	28
Conclusions.....	33

3.	Molecular $\chi^{(2)}$ Gratings Inscribed with Electron Beam Lithography	34
	Introduction.....	34
	Surface Layer Preparation.....	35
	Surface Second Harmonic Diffraction	37
	Conclusions.....	43
4.	Whispering Gallery Microresonators for Second Harmonic Light Generation from a Low Number of Small Molecules.....	44
	Introduction.....	44
	NL Molecular Surface Layer Preparation.....	45
	NL Pattern Printed on the Sphere Surface for Quasi-Phase Matching.....	47
	Surface SHG in the WGM	50
	Temporal Walk-off Compensation between Fundamental and SH Pulses.....	55
	SHG and Sphere Q-factor.....	58
	SHG and Molecular Density	62
	SHG from the smallest Number of Molecules	64
	Conclusion	70
	Conclusion and Outlook.....	71
	Bibliography.....	75
	Table of Figures	88

Abstract

In recent years, it has been proposed that circular microresonators may become an important element in the core of many photonic devices. The high Q-factors seen in fused silica micro-spheres and micro-toroids for light coupled in the whispering gallery modes (WGMs) inside the micro-resonator led to many new developments in a diversity of fields. Indeed, WGM micro-resonators have found applications in laser oscillation, optical filtering, bio and chemical sensing, frequency stabilization, quantum electrodynamics experiments, nonlinear parametric conversion and in many other light-matter interaction processes where light recirculation is an essential ingredient. For second and third order nonlinear optical phenomena a high-Q micro circular cavity is an ideal framework to lower the light intensity or material density and still obtain a measurable interaction. This may become particularly useful when the nonlinear interaction is considered on the sphere surface because at an interface centro-symmetry is always broken. In this thesis, we approach the problem of obtaining second harmonic generation (SHG) with the smallest

amount of material possible. Our goal is to demonstrate that WGMs in micro-sphere resonators are an optimal option to consider such type of non-linear interaction. SHG from a small amount of material may find interesting applications in high sensitivity unmarked detection of low numbers of very small objects such as molecules, viruses or other types of nano-particles.

The different experimental and theoretical developments we implemented to achieve such goal are reported in the four chapters of the current thesis. In chapter 1 we introduce basic concepts of spherical micro-resonators and their interest. Theoretical aspects of light propagation and nonlinear light generation in the whispering gallery modes in such micro-resonators are discussed in Chapter 2. A new method to obtain patterns of non-linear material is presented in Chapter 3. In Chapter 4, the developments presented in the previous chapters are combined to obtain second harmonic generation in the whispering gallery modes of microspheres. In this chapter we report the design and fabrication of a nonlinear spherical resonator to experimentally measure SHG from molecules deposited on its surface. Such nonlinear interaction is quasi-phase matched by implementing the periodical patterning reported in Chapter 3 on a molecular layer deposited on the surface of a micro-sphere. By coupling laser light pulses at the fundamental frequency into the whispering gallery modes of the high-Q spherical micro-resonators we demonstrate that a signal at the second harmonic (SH) frequency can be measured when less than 100 molecules contribute in the nonlinear interaction. Finally, applications of such type of generation in highly sensitive sensing are discussed.

Resumen

En años recientes los microresonadores circulares han sido propuestos como un elemento central para formar parte de muchos dispositivos fotónicos. El alto factor de calidad observado en microesferas o microtoroides de sílice cuando la luz se propaga en modos “whispering gallery” (WG) ha dado lugar a un gran número de nuevos desarrollos en campos muy diversos. En efecto, los micro resonadores con modos WG han encontrado aplicación en la oscilación laser, en el filtrado óptico, en sensores bioquímicos, como estabilizadores de frecuencia, en experimentos de electrodinámica cuántica, en la conversión paramétrica no lineal y en muchas otros procesos donde la recirculación de luz es un ingrediente esencial para su interacción con la materia. En fenómenos ópticos no lineales de segundo y tercer orden, la micro cavidad circular con un alto factor de calidad constituye una estructura ideal para poder obtener una interacción medible incluso cuando se consideran pequeñas intensidades de luz o bajas densidades de materia. Esto puede

resultar particularmente útil en la superficie de la microesfera ya que en la interface entre dos materiales se rompe la simetría de inversión incluso cuando los materiales son centro simétricos. En esta tesis abordamos la generación de segundo armónico con una cantidad mínima de material. Nuestra meta es demostrar que los modos WG en resonadores de microesfera son una opción óptima para poder considerar este tipo de interacción no lineal. La generación de segundo armónico con una cantidad muy pequeña de material puede encontrar aplicaciones interesantes en la detección de muy pocos objetos pequeños tales como moléculas, virus o cualquier otro tipo de nanopartículas.

Los diferentes desarrollos experimentales y teóricos que implementamos para alcanzar nuestro objetivo están explicados en los cuatro capítulos de esta tesis. En el Capítulo 1 introducimos conceptos básicos de microresonadores esféricos y su interés. Aspectos teóricos de la propagación y generación no lineal de luz de los modos WG en dichos resonadores se discuten en el Capítulo 2. Un método nuevo para generar patrones de material no lineal se presenta en el Capítulo 3. En el Capítulo 4, los desarrollos de los capítulos previos presentados se combinan para implementar la generación de segundo armónico en los modos WG de las microesferas. En este capítulo reportamos el diseño y la fabricación del resonador esférico no lineal para llegar a medir experimentalmente la generación de segundo armónico de las moléculas depositadas en su superficie. Dicha interacción no lineal se obtiene en la configuración “quasi-phase matched” implementando el mecanismo de escritura de patrones reportado en el Capítulo 3, sobre una capa molecular depositada en la superficie de la microesfera. Mediante el acoplamiento de pulsos de luz láser a la frecuencia fundamental en los modos WG de un microresonador esférico con un alto factor de calidad Q , demostramos que la señal a la frecuencia de segundo armónico puede ser medida, menos de 100 moléculas contribuyen a esta

interacción no lineal. Finalmente, se discuten aplicaciones de ese tipo de generación para la detección altamente sensible.

Resum

En anys recents els micro ressonadors circulars han estat proposats com un element central per a formar part de molts dispositius fotònics. L'alt factor de qualitat observat en microesferes o microtoroides de sílice quan la llum es propaga en modes “whispering gallery” (WG) ha donat lloc a un gran nombre de nous desenvolupaments en camps molt diversos. En efecte, els micro ressonadors amb modes WG han trobat aplicació en l'oscil·lació làser, en el filtrat òptic, en sensors bioquímics, com estabilitzadors de freqüència, en experiments d'electrodinàmica quàntica, en la conversió paramètrica no lineal i en moltes altres processos on la re-circulació de llum és un ingredient essencial per la interacció amb la matèria. En fenòmens òptics no lineals de segon i tercer ordre, la microcavitat circular amb un alt factor de qualitat constitueix una estructura ideal per poder obtenir una interacció mesurable fins i tot quan es consideren petites intensitats de llum o baixes densitats de matèria. Això pot resultar particularment útil en la superfície de la microesfera ja que en la interface entre dos materials es trenca la simetria d'inversió fins i

tot quan els materials són centro-simètrics. En aquesta tesi abordem la generació de segon harmònic amb una quantitat mínima de material. La nostra meta és demostrar que els modes WG en ressonadors de microesfera són una opció òptima per poder considerar aquest tipus d'interacció no lineal. La generació de segon harmònic amb una quantitat molt petita de material pot trobar aplicacions interessants en la detecció de molt pocs objectes petits tals com molècules, virusos o qualsevol altre tipus de nanopartícules.

Els diferents desenvolupaments experimentals i teòrics que implementem per aconseguir el nostre objectiu estan explicats en els quatre capítols d'aquesta tesi. Al Capítol 1 introduïm conceptes bàsics de microresonadores esfèrics i el seu interès. Aspectes teòrics de la propagació i generació no lineal de llum en els modes WG en aquests ressonadors es discuteixen al Capítol 2. Un mètode nou per generar patrons de material no lineal es presenta en el Capítol 3. En el capítol 4, els desenvolupaments dels capítols previs presentats es combinen per implementar la generació de segon harmònic en els modes WG de les microesferes. En aquest capítol reportem el disseny i la fabricació del ressonador esfèric no lineal per arribar a obtenir experimentalment la generació de segon harmònic de les molècules dipositades a la superfície. Aquesta interacció no lineal s'obté en la configuració “quasi - phase matched” implementant el mecanisme d'escriptura de patrons reportat en el capítol 3, sobre una capa molecular dipositada a la superfície de la microesfera. Amb l'acoplament de polsos de llum làser a la freqüència fonamental en els modes WG d'un microresonador esfèric amb un alt factor de qualitat Q demostrem que la senyal a la freqüència de segon harmònic pot ser mesurada, quan menys de 100 molècules contribueixen a aquesta interacció no lineal. Finalment es discuteixen aplicacions d'aquest tipus de generació per a la detecció altament sensible.

1. Introduction

Circular Optical Microresonators as Sensors

Circular optical microresonators have been considered for the study of linear, nonlinear, quantum optical, optical engineering and integrated optical studies leading to a significant impact scientific and several technological applications (1). Circular microresonators are used as laser oscillators, filters, biosensors, frequency stabilizers, in quantum electrodynamics experiments, nonlinear parametric conversion and in many other optical processes where light recirculation is needed (2). Some authors have indicated that circular optical microresonators may become the building block for the next-generation of optoelectronic devices with a compact-size, operating at low-power provided light is strongly confined.

Such circular microresonators exhibit high Q factors which result in very sharp resonances for the light that propagates in the so-called whispering gallery modes (WGM) (3). In passive devices, small changes in the properties of the surface of the resonator would result in detectable displacements in the frequency of the resonant modes (4), (5), (6), (7), (8). Such displacements in the frequency of the resonant modes have been used to detect the presence of single nanoparticle or single viruses (8), (9), (10), (11). These results triggered the development of new theoretical work with the aim to fully elucidate the physical origin of such tiny displacements (12). On the other hand, to enhance the sensitivity of such passive devices it has been proposed that the alternative configurations based on a splitting resonator can be used to detect the presence of nanoparticles (13), (14). Combination of circular microresonator and a reference interferometer has also been considered to measure a wavelength shift produced by a nanoparticle (10). In many of such cases, however, the passive nature of the underlying physics limits the applicability of the detection procedure to sense relatively large molecules or objects. In active devices one may take advantage of the same high Q factors to obtain laser light generation (1), (15), (16), (17) or enhance nonlinear interactions (18), (19). As schematically shown in **Figure 1-1**, an active optical resonator can increase the effective Q-factor. For instance, a resonator with optical gain the loss can be compensated by the gain medium and effectively reduce the linewidth and improve the sensitivity and detection limit (20). Finally, as we shall see in the next section active resonators where the interaction is nonlinear have also been considered by many different research groups.

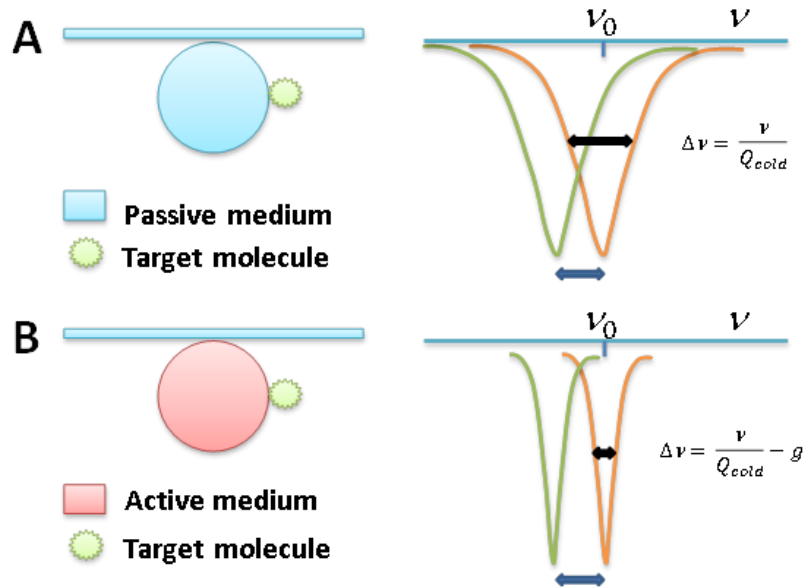


Figure 1-1 The binding of molecules on the surface of a resonator shifts the resonant frequency. (A) A passive resonator has less resolution than (B) an active resonator. The reactive shift method can be enhanced through optical gain by improving the minimum detectable resonant shift (20), where $\Delta\nu$ is the resonance linewidth calculated from cold cavity Q factor and the gain g is the lasing mode at the WGM resonant frequency ν_0 .

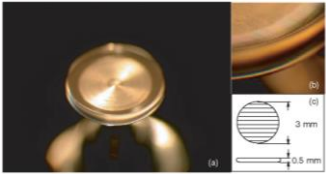
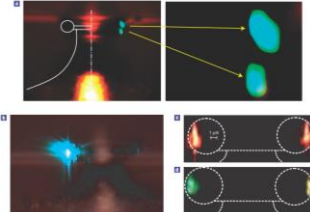
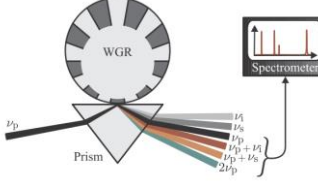
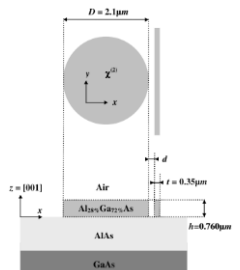
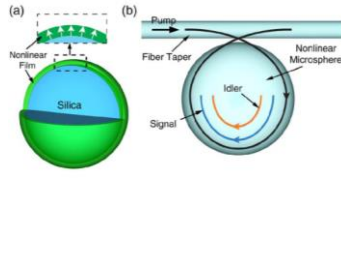
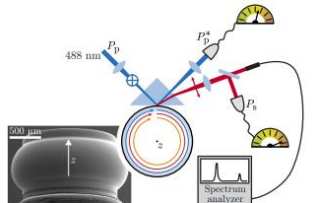
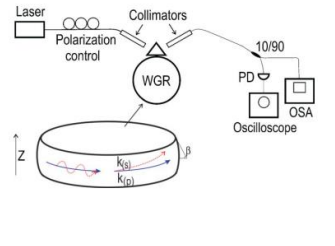
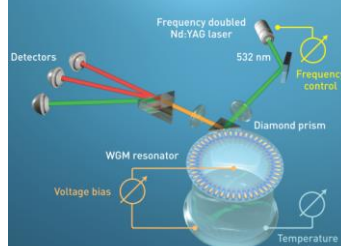
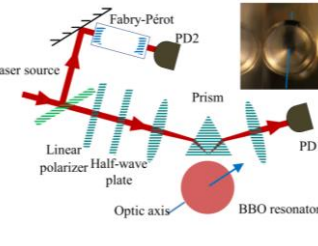
Nonlinear Optics in Circular Microresonators

In quadratic nonlinear optics an efficient energy transfer in between the interacting waves requires the inversion symmetry to be broken and some kind of phase matching mechanism. Traditionally, birefringent non-centrosymmetric inorganic crystals have been used to efficiently up- or down-convert the frequency of an incoming laser beam. To match the phase velocities, an alternative route to birefringence is to introduce a periodic modulation of the index of refraction in the same direction as the beam propagation leading to what is known as quasi-phase matching (21). Birefringence and quasi-phase matching have been effectively used to obtain laser light at almost any frequency within the ultraviolet (UV), visible and infrared ranges. There are, however, many other applications that would benefit from a mechanism capable of generating light from a non-fluorescent

source but cannot afford to be implemented in dense matter, birefringent, or non-centrosymmetric configurations.

At the interface between two media the inversion symmetry is always broken. In such configuration, any molecule, fluorescent or non-fluorescent, can in principle exhibit a measurable second-order nonlinear response to an optical signal. The surfaces of spherical or other types of circular micro-resonators may potentially be an optimal interface to consider such type of nonlinear interaction. However, to achieve an efficient non-linear interaction in a circular micro resonator is, indeed, a rather challenging task. In addition to have resonant modes at ω and 2ω or 3ω , one must phase match the two interacting waves. It has been theoretically shown that within circular microresonators perfect phase matching may be achieved using different radial WGM for the fundamental and harmonic fields (22), (23), (24), (25), (26). As shown in (25) and as discussed in the next chapter of the current thesis, phase matching amounts here to conservation of angular momentum. This happens however only for specific radii and the overall overlap of the two interacting waves is limited. Quasi-phase matching is an alternative route that offers, in principle, more flexibility (22), (25), but it was until recently regarded as technically very difficult to implement. Some examples that, prior to the end of the writing of the current thesis, have considered a nonlinear parametric interaction in circular micro-resonators are shown in Table 1.

Table 1. Examples for microcavities that have been utilized nonlinear optics for parametric processes.

		
<p>2004, Toroidal WGM cavity made of periodically poled lithium niobate for SHG (27).</p>	<p>2007, Visible continuous emission from a silica microphotonic device by third-harmonic generation (28).</p>	<p>2011, Highly tunable low-threshold optical parametric oscillator (OPO) in radially poled whispering gallery resonators (29).</p>
		
<p>2006, WGM analysis of phase-matched doubly resonant with AlGaAs micro disk (23).</p>	<p>2008, Second order parametric processes in nonlinear silica microspheres (30)</p>	<p>2012, Blue-pumped WGM OPO (31)</p>
		
<p>2007, Parametric oscillations in a WGR (19).</p>	<p>2010, Sub and SHG using WGM, continuous wave light (26) (32).</p>	<p>2012, WGM PO pumped at 488 nm to cover visible range. (33).</p>

Objectives and Outline

The main goal of this thesis is to demonstrate that WGMs in micro-sphere resonators are an optimal option to consider surface non-linear interaction because, as indicated above, at an interface centro-symmetry is always broken. In this thesis, we approach the problem of obtaining SHG with the smallest amount of material possible. SHG from a small amount of material may find interesting applications in high sensitivity unmarked detection of low numbers of very small objects such as molecules, viruses or other types of nanoparticles.

The different experimental and theoretical developments we implemented to achieve such goal are reported in the next three chapters of the current thesis.

In Chapter 2 we provide an overview of WGM propagation in fused silica spheres and surface nonlinear wave mixing on the surface of such spheres. Phase and quasi-phase matching conditions for the SHG in the WGM are thoroughly discussed.

In Chapter 3 we demonstrate a new procedure to fabricate surface patterns of nonlinear material using electron irradiation. We show that such irradiation quenches the second-order nonlinearity of molecules adsorbed on a quartz substrate. Molecular second-order susceptibility gratings via electron beam lithography are presented for second harmonic diffraction intensity measurements.

Finally, in Chapter 4 we report the design and fabrication of a nonlinear spherical resonator to experimentally measure SHG from molecules deposited on its surface. Such nonlinear interaction is quasi-phase matched by periodically patterning the surface molecular layer.

Laser light pulses at the fundamental frequency are coupled into the whispering gallery modes of the high-Q spherical micro-resonators. By previously stretching the pulses to prevent walk-off, the interaction time could be used many times to build up a light signal at the second harmonic (SH) frequency, and the number of molecules needed for the generation could be brought down to a level at which less than 100 molecules were required to measure a detectable change in the generated light.

2. Whispering Gallery Modes and Surface SHG.

Introduction

Whispering gallery modes (WGM) have been studied extensively since 1908 when the theory of light scattering from dielectric spheres was established by Mie (34). In this chapter, I will briefly review WGM propagation in such kind of micro-resonators and surface second order nonlinear light generation for high Q microspheres when considering a uniform nonlinear susceptibility covering such dielectric sphere (35).

Circular Optical Microresonators

An optical resonator may be characterized by two key parameters: modal volume (V) and quality factor (Q) that represent the spatial and temporal light confinement, respectively.

The resonator capacity to circulate and store light is in the Q-factor while the volume occupied by the confined optical mode is known as the Mode Volume (36). As indicated in the previous chapter high Q microcavity leads to a multiple recirculation of optical power, which may be used to maintain laser oscillation, to increase the effective path length in spectroscopic studies, to improve the resolution in interferometry measurements or to enhance parametric oscillations in wave mixing interactions (19), (3). Reduction of modal volume is required for the detection of a few numbers of molecules (37) or to control the spacing of resonant frequencies for optical telecommunications (38).

Several circular structures such as spheres (39), toroids (40), disks (41) and cylinders (42), have been shown to support very high-Q WGM. WGM light propagation in such structures can be understood as closed circular beams supported by total internal reflections from the boundaries of the cavity. For the case of a spherical resonator, the field intensity distribution of a high Q WGM may look like a ring of light strongly confined as schematically shown in **Figure 2-1**. From a geometrical optics perspective such WGM may be seen as a zig-zag path resulting from continuous quasi-total internal reflections as shown schematically in **Figure 2-2**.

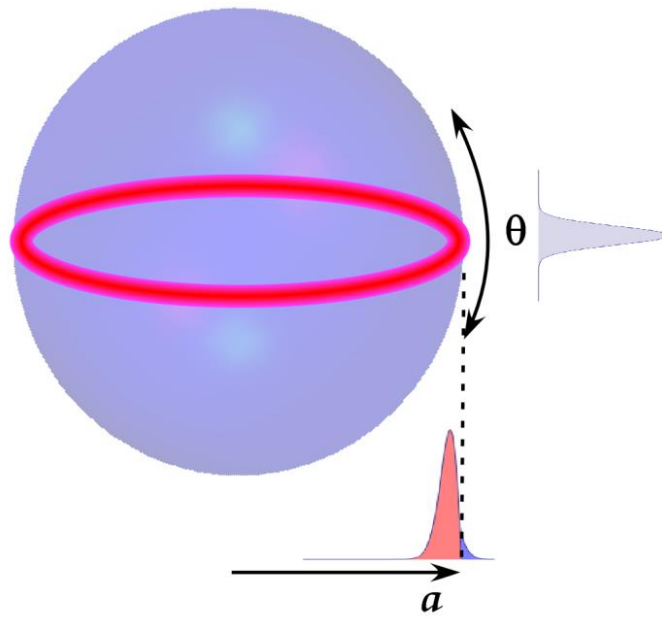


Figure 2-1. Schematic representation of a WGM mode when the sphere radius is much higher than the resonant wavelength.

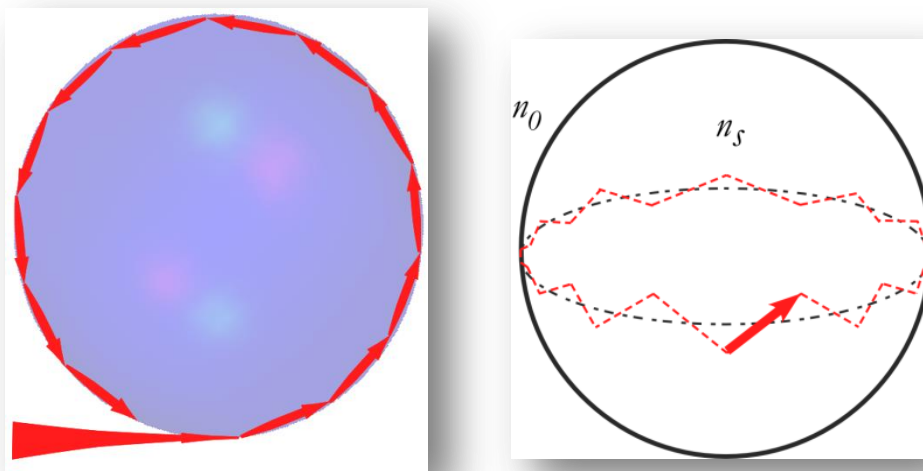


Figure 2-2. From ray optics WGM modes can be understood as a zig-zag path resulting from multiple total internal reflections. The refractive index of the sphere is n_s and the one from the surrounded media is n_0 .

Fused Silica Spherical Microresonators

The technologic progress brought by the laser, light detectors and optical fibers have contributed to the fast growing of information systems with the light as the information carrier. Initial fiber optic losses of 1000 dB/Km were lowered in 1970 and subsequent years to 20 dB/Km and set to 0.2 dB/km in 1979 (43), only limited by the intrinsic losses of Rayleigh scattering (44). The pure fused silica used in optical fiber can also be used to produce spherical cavities to trap light easily and at low cost (39), (45), (46), (47). A fused silica sphere is able to effectively trap light when the surrounding medium is air.

A low attenuation of the light propagation in a fused silica sphere is the main requirement to observe high quality factors in the order of $Q \sim 10^{10}$, (48) when, for instance, using light at 633nm. At a given sphere radius, the maximum Q that can be reached is typically limited by intrinsic material losses and the scattering losses from imperfections or surface roughness that are created mainly in the manufacturing process. This is why highly transparent materials with a large degree of purity provide the possibility to achieve the highest quality factors (3). Light trapping becomes more efficient as the radius of curvature of the sphere increases relative to the wavelength of the such light (36).

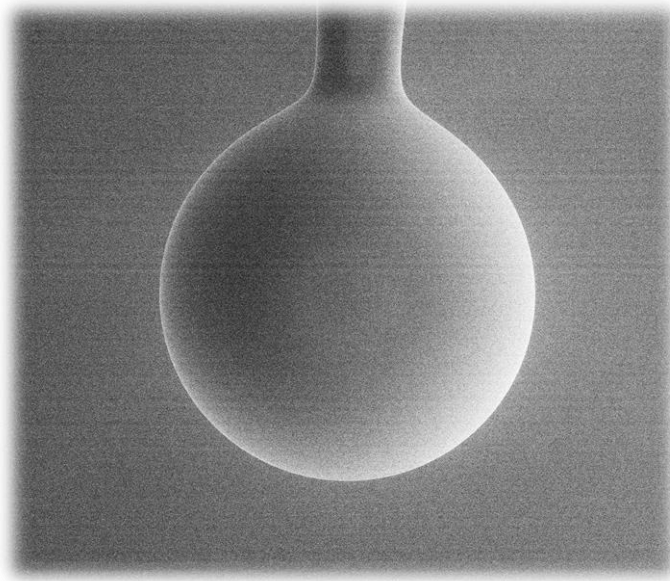


Figure 2-3. Fused silica sphere microcavity image from a Scanning Electron Microscopy and the glass stem that is used to support and manipulate such microcavity.

Melting the tip of a fused silica optical fiber can produce a high Q microresonator of this solid amorphous material with small optical attenuation (49) without quality post processing. The most interesting advantages of fused silica respect to crystalline microresonators is that a polishing procedure is not requires and that smaller size devices can be fabricated (26), (27), (19) , (50). A fused silica microsphere as shown in **Figure 2-3** with the glass stem that is used to support and manipulate such microcavity.

Coupling Light in a Microsphere

An efficient and robust coupling to WGMs is a very relevant issue when considering any practical application of WGRs (3). A tapered fiber adjacent to the microsphere is considered to be one of the most efficient coupling procedures to excite WGM in such microsphere (51). An efficient coupling is achieved when overlapping the evanescent fields

from the fiber and the WGM leakage from the microsphere (52), (45), (53). A taper fiber is typically fabricated heating and pulling standard optical fibers (54). Such tapered fiber is used as the channel to couple in/out laser light to/from the circular resonator. The coupling system set-up is shown in the **Figure 2-4**.

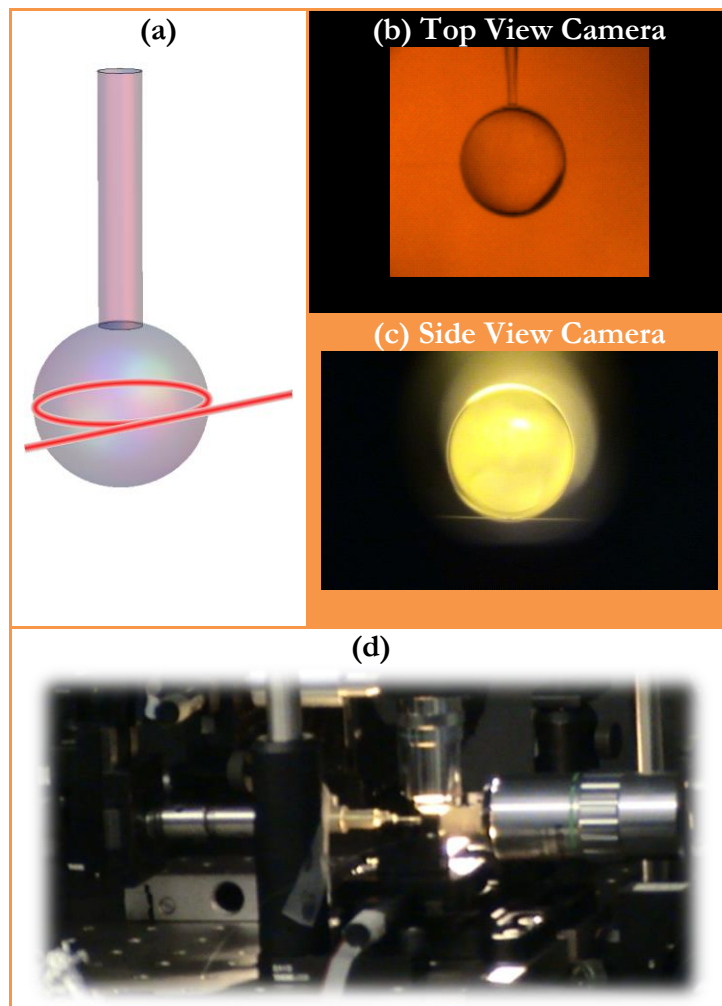


Figure 2-4. a) Scheme of a tapered fiber and microsphere coupling system. Top view b) and side view c) of coupling system and experimental set-up d).

We use fiber-sphere system to efficient controllable coupling, the critical requirement of feasibility of practical applications of the resonators can only be achieved via the near field

of a WGM where in the context of critical coupling, it filters all other waveguide modes very efficiently, save the fundamental, at both the input and the output (3) . It has been shown that critical coupling for visible and near IR is possible when using tapered fibers close to $1\mu m$ in diameter (55), (56). The tapered fiber must be carefully designed and positioned to inject a maximum amount of light into the micro-cavity (57), (58), (52), (59), (56), (60), (61), (62), (63) .

Understanding the WGM Propagation of Light Inside a Micro-Sphere

To describe light propagation and nonlinear light generation at the sphere surface, one must extend the classical Mie theory to include a surface nonlinear polarization (25). With a dielectric sphere of radius a in a vacuum environment, Maxwell's equations can be written as:

$$\nabla^2 E - \frac{1}{c^2} \frac{\partial^2 E}{\partial t^2} = \mu_0 \frac{\partial^2}{\partial t^2} (P_L + \delta(r - a)P_{NL}), \quad (2-1)$$

$$\nabla^2 H - \frac{1}{c^2} \frac{\partial^2 H}{\partial t^2} = -\nabla \times \frac{\partial}{\partial t} (P_L + \delta(r - a)P_{NL}), \quad (2-2)$$

$$\nabla \cdot E = 0, \quad \nabla \cdot H = 0, \quad (2-3)$$

where P_L is the linear polarization and P_{NL} is a surface nonlinearity. These vectorial equations can be turned into scalar ones thanks to the identity

$$\mathbf{r} \cdot (\nabla^2 \mathbf{E}) = \nabla^2(\mathbf{r} \cdot \mathbf{E}) - 2\nabla \cdot \mathbf{E} = \nabla^2(\mathbf{r} \cdot \mathbf{E}). \quad (2-4)$$

This yields

$$\left(\nabla^2 - \frac{1}{c^2} \frac{\partial}{\partial t^2} \right) (\mathbf{r} \cdot \mathbf{E}) = \mu_0 r \frac{\partial^2}{\partial t^2} (P_L + \delta(r - a)P_{NL}), \quad (2-5)$$

$$\left(\nabla^2 - \frac{1}{c^2} \frac{\partial}{\partial t^2} \right) (\mathbf{r} \cdot \mathbf{H}) = -\mathbf{r} \cdot \left[\nabla \times \frac{\partial}{\partial t} (P_L + \delta(r - a)P_{NL}) \right], \quad (2-6)$$

In the absence of P_{NL} both equations have separable solutions of the form $Y_{lmp}(\theta, \varphi)g_{lmp}(r)e^{-i\omega t}$, where $Y_{lmp}(\theta, \varphi)$ is a spherical harmonic and $g_{lmp}(r)$ is a spherical Bessel function (25). The indices l , m , and p are, respectively, the orbital, azimuthal, and radial numbers. Solution in the wave propagation equation is possible with the angular and radial variables separation, combination of the numbers l , m , p for each TE or TM polatization that gives the propagation configuration of the resonant modes inside the circular cavity. Furthermore, if $\mathbf{r} \cdot \mathbf{H} = 0$, the solution is transverse magnetic and if $\mathbf{r} \cdot \mathbf{E} = 0$, the solution is transverse electric. As an example, some field intensity distributions for such type of solutions corresponding to an orbital number $l \gg 1$, $l = m$, and a low radial numbers are depicted in **Figure 2-5** and in **Figure 2-6** field intensity distributions are shown for the lowest radial number when $|m| \leq l$, for three different angular field distributions (3).

As it will be discussed below, in our experiments we used a 5 THz bandwidth femtosecond laser source. Provided the size of the fabricated spheres, the light from the laser pulses was coupled simultaneously into several resonant modes of the sphere. We observed an

extended light distribution (cf. **Figure 2-7**) that seems to support the idea of control such multiple resonant mode coupling.

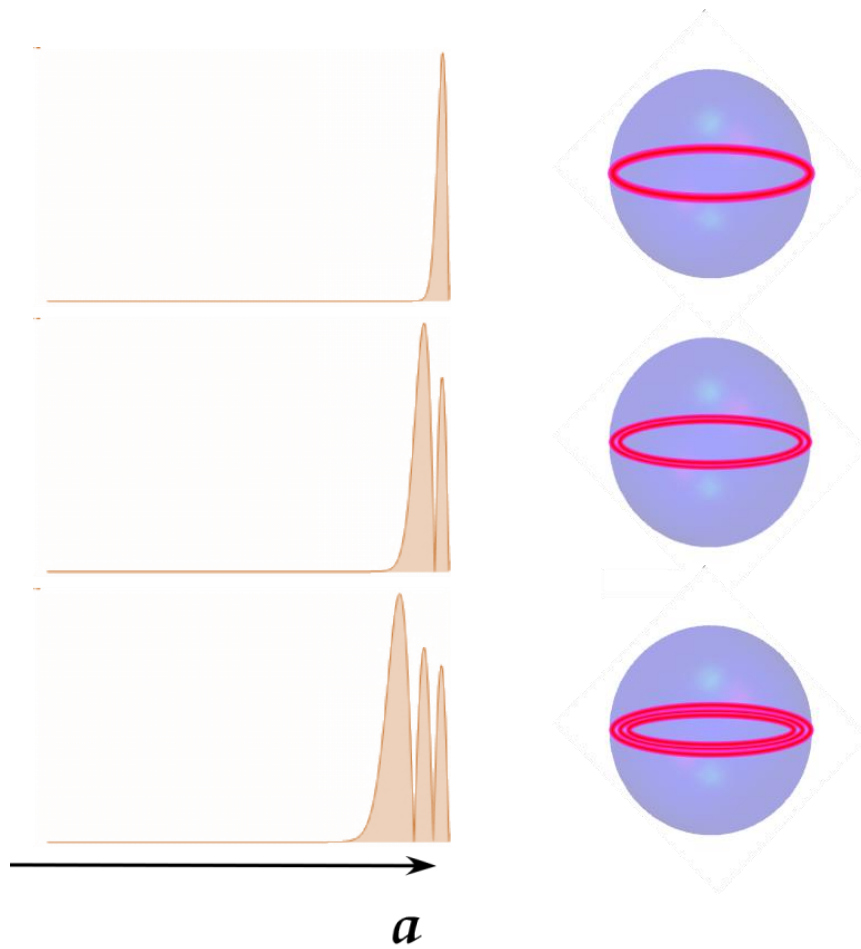


Figure 2-5. Schematic representation of the radial distribution intensity inside the fused silica microsphere when $p = 1, 2, 3$ and $l = m$.

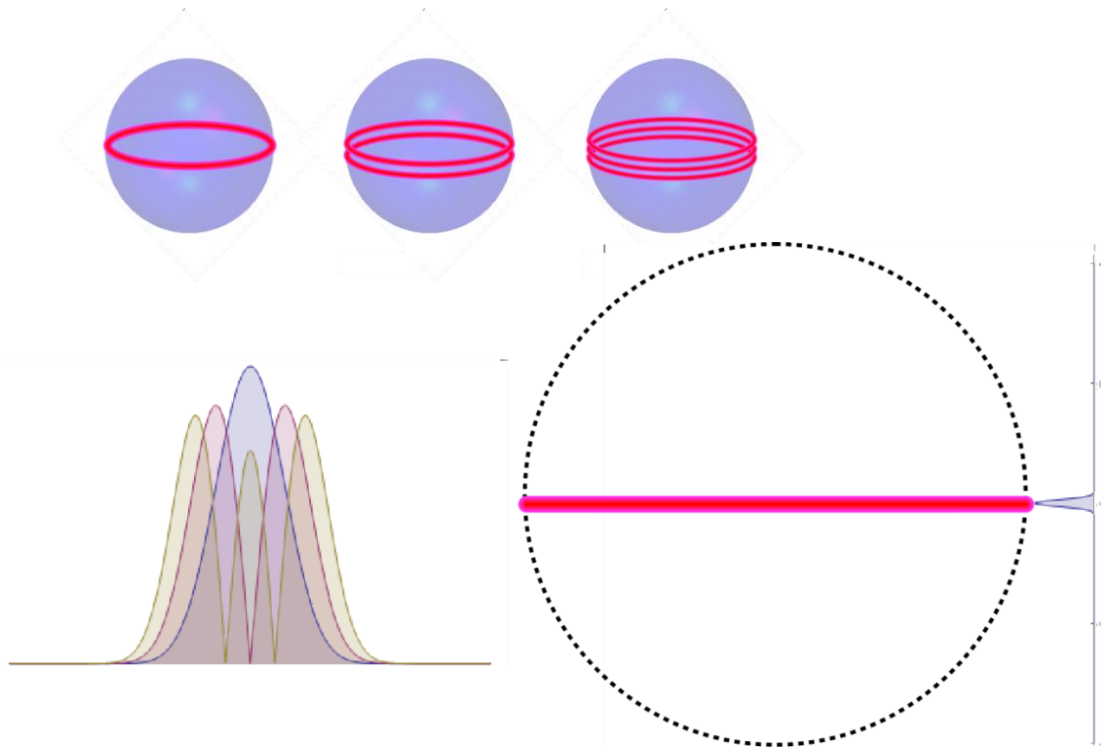


Figure 2-6. Normalized intensity distribution in angular direction of a microsphere with $180\mu m$ in radius, where $p = 1$ and $l - |m| = 1$ (blue), 2(red) and 3(green).

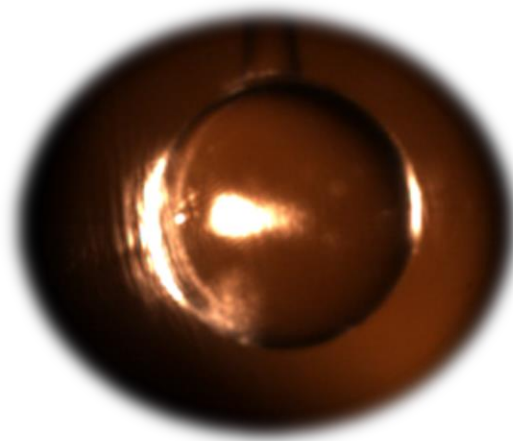


Figure 2-7. Picture of the light scattered out from the sphere surface. Extended light distribution that seems to support the idea of multiple resonant mode coupling.

Surface SHG in Whispering Gallery Modes

To consider SHG from the surface of the sphere, we assume a light wave at frequency ω being injected in a dielectric sphere with radius a via a tapered fiber. This mode of injection excites a WGM in the sphere. Through a surface second-order nonlinearity, one hopes to generate light at frequency 2ω . This requires the existence of another WGM near this frequency and to fulfill some phase-matching condition. Knowing the spherical modes $\mathbf{E}_\omega(\mathbf{r})$ and $\mathbf{E}_{2\omega}(\mathbf{r})$ that are most likely to participate to the second order nonlinear dynamics, we can seek to express the field as:

$$\mathbf{E} = \alpha_1(t)\mathbf{E}_\omega(\mathbf{r})e^{i\omega t} + \alpha_2(t)\mathbf{E}_{2\omega}(\mathbf{r})e^{i2\omega t} + c. c., \quad (2-7)$$

The problem can be solved once the slow varying amplitudes $\alpha_i(t)$ are determined. A convenient way to normalized α_i is such that $|\alpha_i|^2$ is the radiated power. Such varying amplitudes may be obtained from:

$$\frac{d\alpha_1}{dt} + \Gamma_1\alpha_1 = i\kappa^*\alpha_1^*\alpha_2e^{-i\Delta\omega t}, \quad (2-8)$$

$$\frac{d\alpha_2}{dt} + \Gamma_2\alpha_2 = i\kappa\alpha_1^2e^{-i\Delta\omega t} \quad (2-9)$$

where $\Delta\omega = \omega_2 - 2\omega_1$ is the detuning between the fundamental and second harmonic WGM resonances, Γ_i are the width of these resonances, and κ is the nonlinear coupling

between the two modes. The calculation of the coupling coefficient κ gives the strength of the frequency conversion. Note that on the surface of a centrosymmetric material, the only nonzero components of the nonlinear susceptibility $\chi^{(2)}$ are $\chi_{\perp\perp\perp}$, $\chi_{\perp\parallel\parallel}$ and $\chi_{\parallel\perp\parallel}$, where \perp and \parallel refer to directions that are perpendicular and parallel to the surface, respectively, as in Refs. (64) and (65) we are assuming uniform nonlinear susceptibility over the dielectric sphere.

Phase Matching and Coherence Length

If the nonlinear susceptibility $\chi^{(2)}$ is uniform over the dielectric sphere when, for instance, light is coupled to the TM field at 2ω via the $\chi_{\perp\perp\perp}$, the coupling κ takes the form:

$$\kappa_{MM} = \chi_{\perp\perp\perp} \iint Y_{LM}^* Y_{l'm'} Y_{lm} \sin\theta d\theta d\varphi, \quad (2-10)$$

Hence, if (lm) and $(l'm')$ correspond to the fundamental and (LM) correspond to the second harmonic, respectively, the integral above vanishes unless:

$$M = m + m', \quad |l - l'| \leq L \leq l + l', \quad (2-11)$$

which are the selection rules for composing angular momenta and are the phase matching conditions for second-order nonlinear processes involving WGM's. Hence, in the present setting, phase matching amounts to conserve the angular momentum of the electromagnetic wave, in contrast to linear momentum for plane wave mixing.

In addition to equation (2-11) , another condition for equation (2-10) not to vanish is that

$$L + l + l' \in 2\mathbb{Z}. \tag{2-12}$$

This corresponds to the conservation of parity of the wave functions with respect to $\theta = \pi/2$.

Applying for example the selection rule above to a TM fundamental mode with $m = l$ and its $M = L$, matching requires $L = 2l$. Such a choice corresponds to WGM's that are maximally concentrated on the equator and which are more naturally excited by a taper fiber. With the phase matching condition $L = 2l$, double resonance requires that $k_{2l,P} = 2k_{l,p}$ where p and P are the radial numbers of the fundamental and second harmonic modes, respectively. In **Figure 2-8**, we examine this possibility graphically for $p = 1$ and various values of P . With the refractive index of silica, a fundamental wavelength around 800 nm and a sphere radius around $58 \mu\text{m}$, we found that it is necessary to assume a radial number $P = 3$ for the second harmonic. This is similar to reference (28). **Figure 2-8** also shows that phase matching and double resonance only occur simultaneously for specific spheres sizes only.

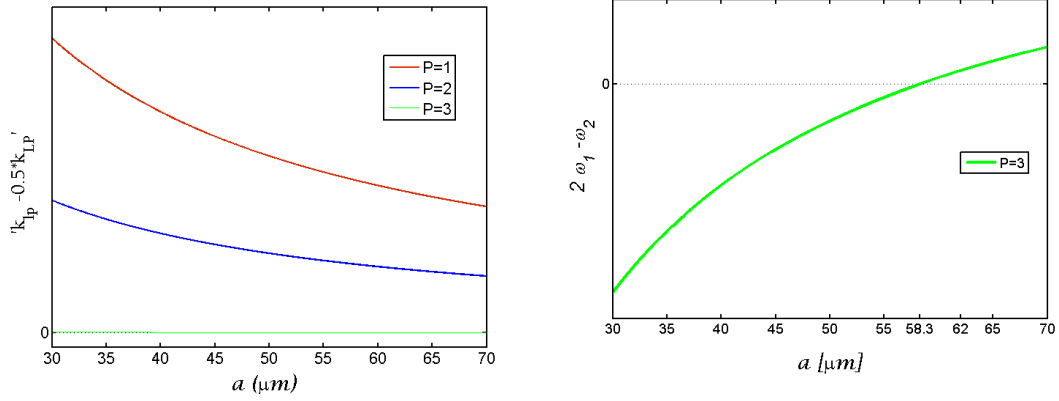


Figure 2-8 Doubly resonant, phase-matched micro-sphere: $(k_{2l,p} = 2k_{l,p})$ a as a function of sphere radius. The choice $L = 2l$ ensures phase matching for whispering gallery modes with $m = l$ and $M = L$. Higher radial wave number must be assumed for the second harmonic. At double resonance ($a \approx 58\mu\text{m}$) the fundamental wavelength is approximately 782nm. In order to draw this curves we assumed a Sellmeyer dispersion formula with $n(\lambda)$ coefficients given in Appendix of (25).

Quasi-Phase Matching for SHG using WGM

From the discussion above it is clear that achieving simultaneously phase matching and double resonance is possible but probably rather difficult in practice. An alternative to phase matching is quasi-phase matching. This can be achieved by covering the sphere only partly with a nonlinear material, or covering it with a periodical pattern of nonlinear material as schematically shown in **Figure 2-9**. In order to cover the sphere correctly it is necessary to determine the coherence length. Focusing on the case $m = l$ and $M = L$, let us restrict the integration in (2-10) to an angular sector of the sphere with arc length ℓ along the equator. We get

$$\kappa_{MM} \propto \sin\left(\frac{L - 2l}{2a} \ell\right) \tag{2-13}$$

Hence, the coherence length along the equator is

$$\ell_c = \frac{\pi a}{L - 2l} \quad (2-14)$$

As one moves away from the equator towards the poles, the coherence length becomes narrower, being maximum at the equator and zero at the poles, then ℓ_c is reduced by a factor $\sin(\theta)$. In other words, optimum quasi phase matching is achievable when the periods resemble the curved surface of an orange slice. At a latitude of polar angle θ on the surface of the sphere, the coherence length is:

$$\ell_c(\theta) = \frac{\pi a}{L - 2l} \sin \theta \quad (2-15)$$

As seen in reference (25) it is possible to obtain an analytical approximation expression for ℓ_c :

$$\ell_c^{-1} \sim \frac{2(n_{s2} - n_{s1})k}{\pi} \left[1 + \frac{n_{s1}^{1/3} - (n_{s2}/4)^{1/3}}{n_{s2} - n_{s1}} \frac{2^{1/3} \alpha_p}{(ka)^{2/3}} \right] \quad (2-16)$$

where α_p is the p root of the Airy function, n_{s2} and n_{s1} are the index of refraction at the sphere for SH and fundamental wavelength, and k is the resonant wavenumber.

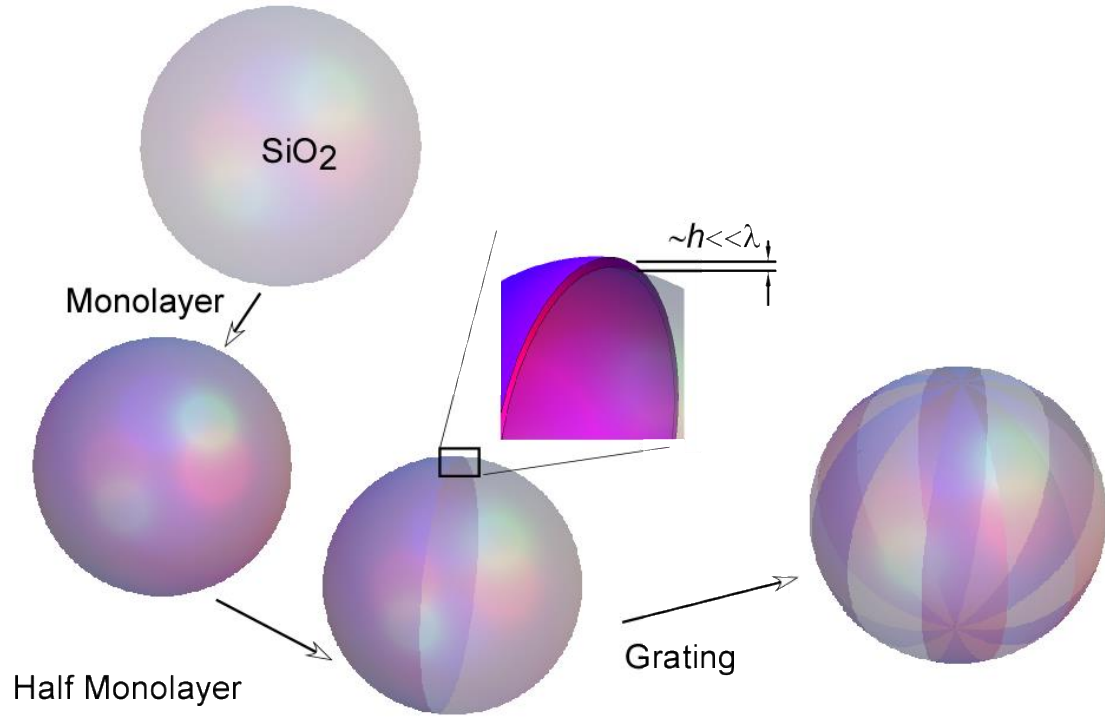


Figure 2-9. Molecular thin layer and grating at the interface of the sphere. Optimum quasi phase matching is achievable when the periods resemble the curved surface of an orange slice.

This formula (2-16) is illustrated in **Figure 2-10** which demonstrates a strong dependence of the coherence length on the sphere size and therefore not only with material dispersion. Note the difference with free space propagation. In the limit of a very large radius ℓ_C^{-1} tends to the bulk value $2(n_{s2} - n_{s1})k/\pi$.

Phase matching or quasi-phase-matching implies double resonance for the two interacting waves. However, the two WGMs taking part in SHG are generally detuned by a finite amount $\Delta\omega_{2,1} = \omega_{L,p} - 2\omega_{l,p}$ from 2:1 resonance. The appropriate values of l and L can be determined from the large- l such asymptotic expansion k_{lp} given in Ref. (25). To

numerically compute ℓ_C as a function of the sphere radius a in **Figure 2-10** we proceeded as follows: We set the fundamental wavelength to 800 nm and chose a radio a and integer l such that we got perfect resonance for that frequency. The values of L were then determined for these radii such that $\Delta\omega_{2,1}$ was less than 10 MHz and the coherent length was deduced from (2-16). The jumps in ℓ_C as a function of the radio seen in **Figure 2-10** results from the discreteness of l and L . Such discrete character combined with the dependence of ℓ_C on the radius underscore the fundamental difference between the present situation and the nonlinear mixing of freely propagating plane waves.

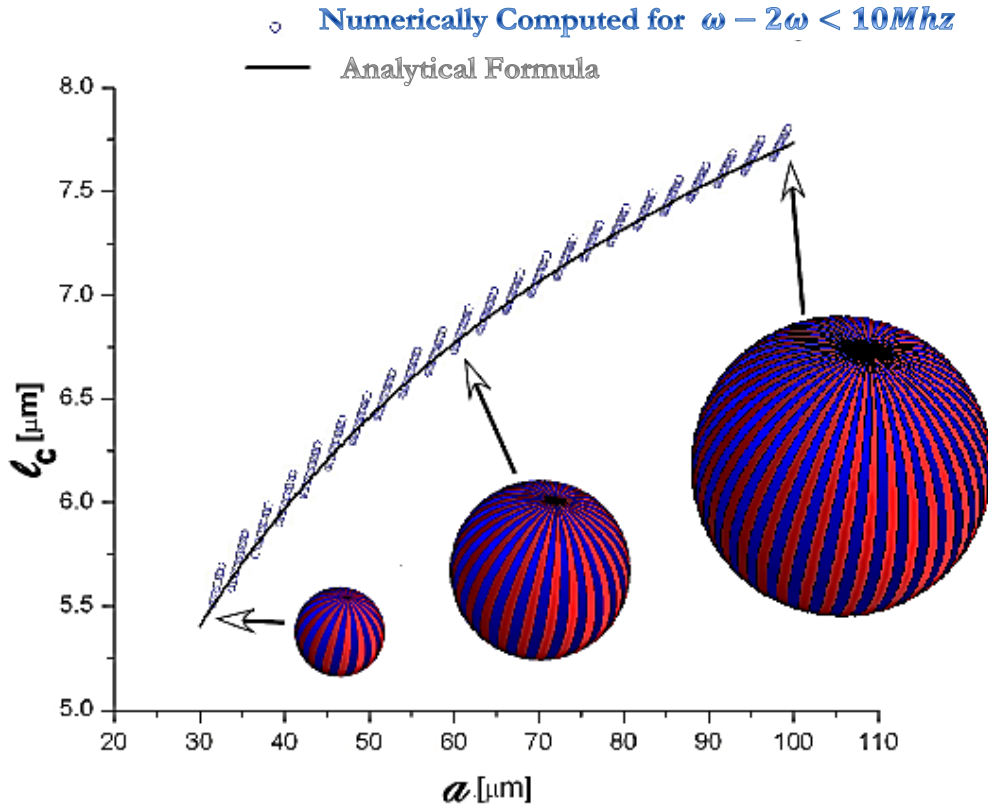


Figure 2-10. Coherence length ℓ_C as a function of sphere radius. Continuous line: analytical formula; circles: numerically computed values from an 8-order asymptotic expansion relating mode frequency and mode orbital and radial numbers (66). The fundamental wavelength is $\lambda = 800\text{ nm}$. Only modes with $m = l, M = L$, and $p = P = 1$ are considered.

Quasi-phase-matching would require to cover the sphere, for instance, with two types of domain slices, one with the nonlinear molecular dipole pointing outwards and the adjacent one with the nonlinear molecular dipole pointing inwards. Such periodic distribution of domains would lead to the largest conversion efficiency possible in such type of microresonators. Note that, from (2-14), in such a periodic configuration, the sphere perimeter is automatically equal to an even number of ℓ_C . Furthermore, quasi phase matching allows one to use the lowest order radial modes for both fundamental and second-harmonic frequency.

Conclusions

In conclusion, we have shown that adequate sphere size and field intensity distribution of a high Q WGM may look like a ring of light strongly confined. Surface nonlinear processes are studied by considering a coupled wave theory to account for the second order nonlinear generation in the whispering gallery modes assuming uniform nonlinear susceptibility over the dielectric sphere. Explicit analytical expressions for the nonlinear coupling are used to establish the phase matching condition as a conservation of the angular momentum of the electromagnetic wave. The problem of perfect phase-matched doubly resonant microresonators can be solved only for some very specific radii between modes with different radial number. As an alternative to perfect phase matching we showed that quasi phase matching is possible by implementing a periodic pattern where the domains or periods resemble the curved surface of an orange slice.

3. Molecular $\chi^{(2)}$ Gratings Inscribed with Electron Beam Lithography

Introduction

High-resolution patterning of ultra-thin films by means of electron-beam lithography is an important tool in nanotechnology, which has been established for several types of organic films on various substrates. The effect of electron-beam irradiation on organic molecules at surfaces is not always known, and usually varies depending on parameters such as substrate temperature, electron kinetic energy and irradiance, and composition of the organic film. Electron irradiation may entail for example total or partial desorption of the film, (67), (68), selective damage to a part of the organic molecule (69), (68) or electron-induced reactions, (70), leading to a modified chemical reactivity or optical activity or, as we show in this chapter, to quenching of the nonlinear optical response of a molecular film.

Systems displaying a periodic modulation of the quadratic nonlinear susceptibility $\chi^{(2)}$ allow simultaneous generation and separation of the second harmonic wave from the fundamental input field (71). Such $\chi^{(2)}$ patterns can operate as couplers (52) into waveguide structures and enable resonance-enhanced wavelength conversion, *e.g.* in nonlinear grating waveguides (72), (73), and are key elements for integrated optics in distributed feedback lasers (74). For quasi-phase-matched second harmonic and difference frequency generation, periodic patterning of the nonlinear optical susceptibility without modification of the linear refractive index is required. Usually, this purely nonlinear modulation is obtained by periodical poling (21).

In this chapter we show that the nonlinear optical activity of an organic molecule may be quenched by electron irradiation. Exploiting this effect, we inscribe periodic $\chi^{(2)}$ patterns in molecular films by means of a scanning electron microscope. The second harmonic diffraction efficiency of the resulting $\chi^{(2)}$ gratings is measured. The relative intensity of the diffraction orders observed agrees with the expectations for a sheet of nonlinear dipoles with a periodic modulation. No linear diffraction is seen. The present method allows to realize any type of two-dimensional $\chi^{(2)}$ pattern with a resolution only limited by the electron beam patterning capabilities.

Surface Layer Preparation

To prepare the $\chi^{(2)}$ grating we exposed thin films of a nonlinear organic chromophore deposited on glass substrates under the electron beam of a scanning electron microscope

(SEM). As we shall see in section the nonlinear optical response of the dye is quenched as a consequence of electron irradiation. This allows us to pattern molecular films of nanometer thickness on a transparent dielectric substrate, thereby achieving a nonlinear $\chi^{(2)}$ grating without modification of the linear refractive index of the medium. Such electron-lithography technique used in this thesis offers several advantages as it produces higher-resolution, precisely aligned, homogeneous patterns, while at the same time allowing for different kinds of two-dimensional patterning also on non-flat surfaces (25).

Thin molecular films of a nonlinear chromophore (crystal violet) were deposited onto microscope quartz slides from an 2.5×10^{-4} molar solution in 1-propanol. For homogeneity and reproducibility, a motorized stage was used for controlled immersion and retrieval, while the choice of solvent enhanced wetting and evaporation in the meniscus region. The substrate was removed from the solution at a constant speed of 1 mm/s using a motorized translation stage. One side of the substrates was carefully cleaned leaving the organic film only on one side. The absorption intensity of the molecular films as measured by extinction spectroscopy indicates that their thickness is of few molecular layers (75).

The electron beam of an SEM designed for lithography purposes was focused, as shown schematically in the inset of **Figure 3-1**, to write a grating onto the molecular film. The electron kinetic energy of the electron beam was set to 10 keV. Preliminary experiments showed that the grating quality was virtually independent upon the impinging electron energy in the range between 5 and 30 keV. During these experiments, we noticed that exposure to SEM illumination in imaging mode, *i.e.* with a relatively low electron dosage, was already sufficient to induce a reduction of second harmonic generation from the molecular film.

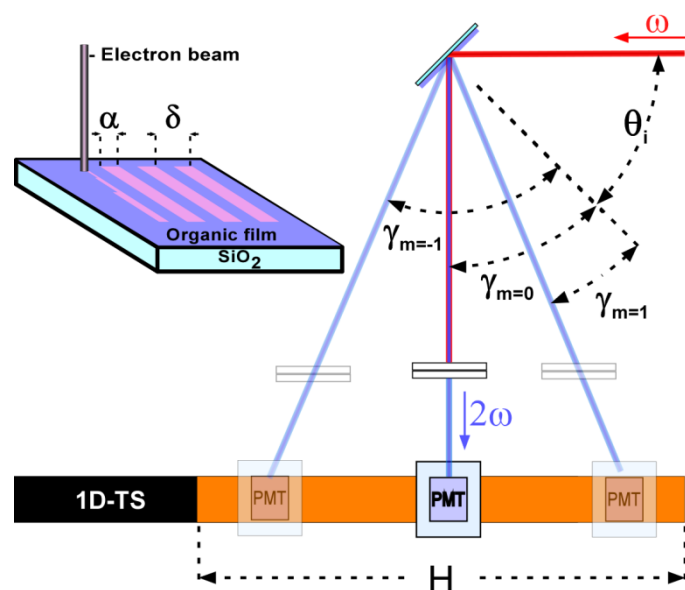


Figure 3-1. Schematic view of the experimental set-up used for measuring the diffracted second harmonic light (TS stands for translation stage). Inset (left): writing of a periodic $\chi^{(2)}$ pattern onto the molecular film by SEM. The nonlinear activity of the molecule is quenched by e-beam irradiation.

To obtain the gratings, the beam was scanned to draw a series of parallel stripes, few microns wide and 2mm long (see inset of **Figure 3-1**), leaving in between a no exposed stripe of either the same width or three times as large, so that the period δ was twice or four times the width α of the irradiated stripe. The non-irradiated film areas constitute a one-dimensional $\chi^{(2)}$ grating. Typical gratings presented in this work had a size of two square millimeters and period ranging from 4 to 40 μm .

Surface Second Harmonic Diffraction

It is known that patterned molecular (and atomic) layers on surfaces may give rise to nonlinear diffraction (76), (77), (78) despite their extremely small thickness compared to the wavelength of the light. Second harmonic diffraction from monolayer gratings has allowed

the study of surface phenomena such as adsorption (78), (79) or diffusion (77), (80), without the interference of substrate effects (76).

For our second harmonic generation experiments we used an amplified Ti:Sapphire laser emitting a 1 kHz train of 150 femtosecond pulses centered at 800 nm in wavelength. The beam was focused using a 50 cm focal distance lens to increase the energy density at the sample, which was placed before the focal point to avoid any damage. The substrate formed an angle of 45° with respect to the laser beam as seen in **Figure 3-1**. The beam size at the position of the sample was of few hundreds microns. The measured surface second harmonic signal at $\lambda = 400$ nm in specular reflection geometry is shown in **Figure 3-2** at different points of a sample containing several gratings. The sample was displaced in steps of 0.025 mm using a micrometric mount in the direction parallel to the plane of the film, *i.e.* at 45° with respect to the laser beam, thus maintaining constant the position of the reflected beam during the scan. Curve (a) was acquired near a pristine region of the film and curve (b) was measured scanning a region with two gratings of same period but different irradiated width α , equal respectively to one half and one fourth of the period ($\delta = 40 \mu\text{m}$), and (c) upon totally irradiated area ratio as shown in the schematics of **Figure 3-2**.

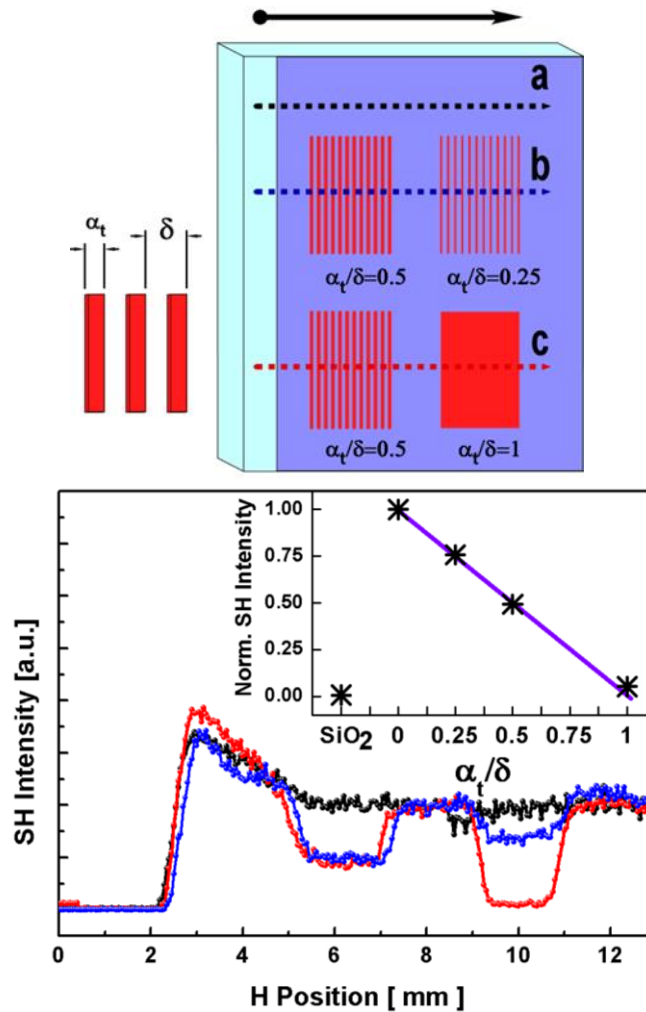


Figure 3-2 Second harmonic (SH) generation scans across different film regions (measured in reflection) as indicated in the schematic view of the experimental set-up: (a) pristine film [dotted black line]; (b) film region with two gratings of same period but different width α of the exposed stripes [dotted blue line]; and (c), film region with one grating of same previous period ratio and upon totally irradiated area ratio [dotted red line].

Both curves display a vanishing intensity on the left-hand side followed, towards the right, by an abrupt onset of the signal in correspondence with the film edge. The almost vanishing signal in the part of the substrate that is not covered by the dye indicates that second harmonic generation from the clean glass surface is almost negligible under our experimental conditions. As visible in the central part of curve (b) in **Figure 3-2**, the inscription of gratings with 25% or 50% irradiated area ratio leads to a lowering of the second harmonic intensity in specular reflection.

The reduction of second harmonic intensity in the grating region is indicative of the presence of damaged molecular areas in the grating region, which shows that spatially-selective irradiation is achieved. For comparison, we have irradiated extended regions of molecular films grown from the same solution using the same SEM settings. In this case, we have seen that the second harmonic signal in reflection is comparable with that of the clean glass substrate, indicating that electron irradiation results in almost total quenching of the non-linear activity of the dye.

As shown in the inset of **Figure 3-2**, the measured second harmonic signal in reflection is approximately proportional to the ratio α/δ , or, which is the same, it is linearly proportional to the average molecular density in the grating region. This is surprising, since from the quadratic dependence of the second harmonic intensity upon molecular density (79), one would expect that the intensity of the zero-order of diffraction in the grating region should be approximately proportional to the square of the non-irradiated area. This discrepancy might be due to a nonlinear interference effect upon generation. It is well known that second harmonic generation is strongly dependent on momentum (or phase) matching conditions; in the present case the generation of second harmonic light from a molecular stripe occurs in the presence of the (near) field generated by neighboring stripes. Given the arbitrariness of the grating period chosen, the phase relationship between the second harmonic fields from different stripes does not give rise to a perfect addition of the second harmonic near-fields, which might explain the less than quadratic dependence of the far field signal upon molecular density. A linear dependence upon domain density is for example observed in the case of second harmonic generation from random 1D structures (75). Further investigation is needed to confirm this hypothesis.

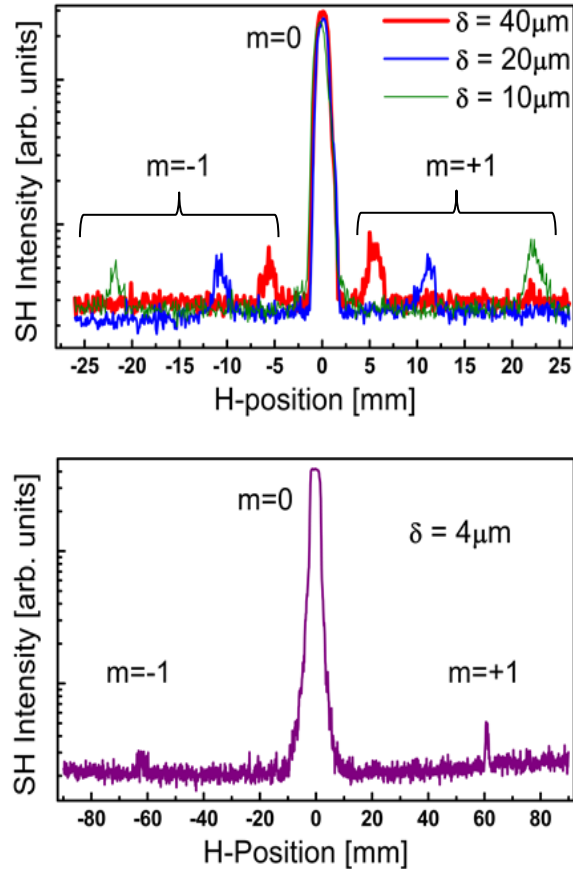


Figure 3-3. Second harmonic diffraction patterns from gratings of different period ((a), $\delta = 40, 20, 10 \mu\text{m}$; (b) $\delta = 4 \mu\text{m}$), with the fundamental beam impinging at 45° . The angular spacing between the diffraction peaks matches the expectations for second harmonic diffraction at a wavelength of 400 nm for the various periods used for the lithography. The intensity of the specular ($m = 0$) order is saturated in the detector.

The second harmonic diffraction patterns obtained with grating periods of $\delta = 40, 20$ and 10 microns and area coverage of 50% are shown in **Figure 3-3**. The diffraction intensities were acquired displacing the detector using a linear motorized stage, as shown in **Figure 3-1**. The angular position of the +1 or -1 diffraction orders agree well with diffraction theory for the second harmonic wavelength where the angular position of the various second harmonic diffraction orders in reflection is given by $\sin\gamma_m = \sin\theta_i + m(\lambda/\delta)$, ($m=0, \pm 1, \pm 2, \dots$). It can be observed that the intensity of the +1 or -1 diffraction orders is approximately the same for all three gratings, which shows that the diffraction efficiency is

not dependent upon the period. This is perhaps not surprising as the second harmonic wavelength used is much smaller than the periodicity of the grating. **Figure 3-3** shows the pattern obtained with a period of $\delta = 4 \mu\text{m}$. The first order of diffraction which indicates a proper grating formation is clearly visible in the figure. Despite the relatively high intensity of the fundamental infrared beam, no linear diffraction was detected for any of the gratings. This demonstrates that the observed diffraction is not a geometrical effect due to surface corrugation induced by the lithography process, but is only the result of the spatial modulation of the hyperpolarizability. From an applied point of view, the absence of diffraction of the fundamental beam is interesting for applications that require the separation of the fundamental and second harmonic beam while avoiding loss of fundamental power into several diffracted orders.

Conclusions

In this chapter, we have shown that electron irradiation effectively quenches the second-order nonlinearity of crystal violet molecules adsorbed on a glass substrate. The exact effect of electron beam irradiation on the molecules is still unknown. The quenching of second harmonic generation could be due to a modification of the electronic or chemical configurations, or to desorption or destruction of the whole molecule. The achieved $\chi^{(2)}$ gratings were characterized by second harmonic diffraction, while no linear diffraction was detected. The high precision in the writing of $\chi^{(2)}$ surface gratings developed in this chapter of the thesis will be used in the following chapter to write a grating on the surface of a sphere. As we will see, e-beam lithography is very convenient in controlling with a high resolution the size and shape of the grating written on the surface of a sphere, which is just a few hundred of micrometers in diameter. Other possible applications of these structures are the phase-matched second harmonic generation in waveguides coated with a nonlinear grating (81), exploiting the patterning capabilities of SEM to implement two-dimensional quasi-phase matching mechanisms (82), or the suppression or enhancement of second harmonic generation at interfaces through Wood's resonance anomalies (83), (84).

4. Whispering Gallery Microresonators for Second Harmonic Light Generation from a Low Number of Small Molecules.

Introduction

In this chapter we report the design and fabrication of a nonlinear spherical resonator to experimentally measure SHG from molecules deposited on its surface. Such nonlinear interaction is quasiphase-matched by periodically patterning the surface molecular layer. Laser light pulses at the fundamental frequency are coupled into the whispering gallery modes of the high-Q spherical microresonators. By previously stretching the pulses to prevent walk-off, the interaction time could be used many times to build up a light signal at the second harmonic (SH) frequency, and the number of molecules needed for the generation could be brought down to a level at which only 50-100 molecules were required to measure a detectable change in the generated light.

NL Molecular Surface Layer Preparation

The NL molecule used in the monolayer for the second harmonic generation experiment was Crystal Violet (CV). The volume occupied by this molecule is 0.02 nm^3 and its molecular weight is 407.99 gr/mol . The chemical composition of the molecule is given in **Figure 4-1**.

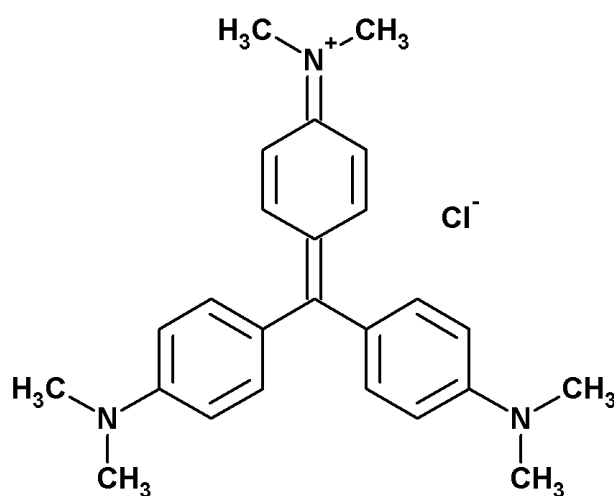


Figure 4-1 . Crystal Violet Molecule.

As it may be inferred from the **Figure 4-1**, CV does not exhibit a permanent dipole moment in the ground state. However, when the molecule is absorbed on the interface, the inversion symmetry is broken and as it has been shown in the past, second harmonic generation in the dipole approximation is possible (85).

The number of molecules on the surface of the sphere can be determined directly from the volume occupied per each molecule in the coating solution. The dip-coating technique is used to obtain a molecular monolayer with a surface density that is proportional to the

concentration of CV in the 1-Propanol solution (86). To demonstrate such linear behavior of the SH signal versus CV concentration we coated, using CV solutions ranging from 1×10^{-5} up to 8×10^{-5} M, 1 mm thick fused quartz flat substrates using the same procedure and conditions that as we will show below were used to coat the sphere. We measured the absorption spectrum of the monolayers obtained using a Perking Elmer LAMBDA 950 UV/Vis/NIR Spectrophotometer. A sample of the absorption spectra taken when the molecules were absorbed on a flat quartz substrate are shown in the inset of **Figure 4-2**. From the peak of absorbance at 597 nm we determined the number of molecules per unit surface in terms of the cross section of CV at the wavelength. As shown in **Figure 4-2**, the surface concentration at a given wavelength grows linearly with the molarity of the original solution. Given such linear proportionality we would be able to estimate from the volume concentration of the solution what the CV surface density at any molarity below 10^{-5} M would be. At very low concentrations the molarity was measured directly using the ultraviolet/visible spectrophotometer and 1-cm path-length cell, we measure for instance, the absorption spectra of the lowest CV concentration in solution for a detectable SH signal. We determined it to be $(1.55 \pm 0.04) \times 10^{-9}$ M provided that the CV cross-section in 1-propanol at 596 nm was $(11.5 \pm 0.3) \times 10^{-16}$ cm². We accurately measured such cross-section using five independently prepared 10^{-7} solutions of CV in 1-propanol. Thus, the CV density on the surface sphere for this concentration was $(7.90 \pm 0.14) \times 10^7$ molecules per cm².

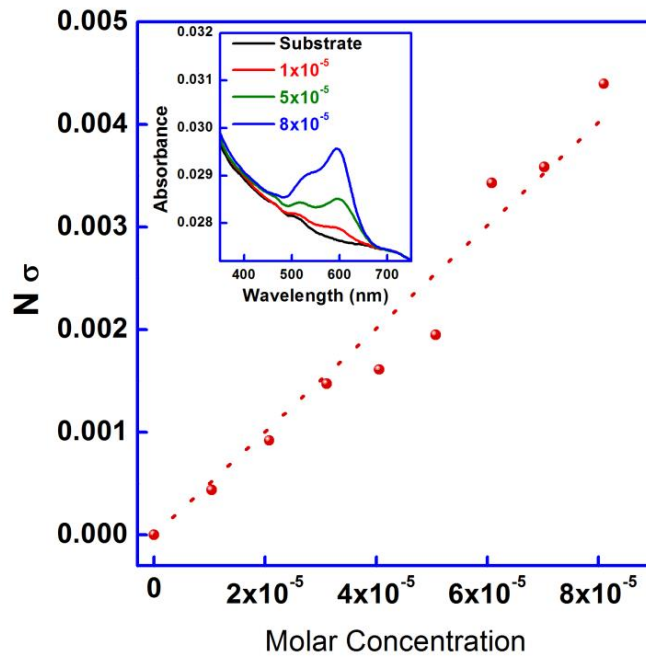


Figure 4-2. The number of CV molecules per unit surface times the cross-section of CV as a function of the molar concentration of the solution used for a coating layer. Inset: absorbance spectra for three monolayers representative of the eight monolayers prepared.

NL Pattern Printed on the Sphere Surface for Quasi-Phase Matching

As explained in Chapter 2 a practical way to achieve phase matching in circular resonators would be to implement periodic distribution of the nonlinear material on the surface. We proved that this is technically feasible using an electron beam gun. As explained in Chapter 3, by launching electrons accelerated under 10kV, we were able to destroy the nonlinear activity of the organic molecules on the surface at will.

As explained in chapter 2 of the current thesis, the design of this pattern must compensate both the material index dispersion and the modal effective index dispersion which depends on the orbital number l . This number is related to the wavenumber in vacuum k and

sphere radius a . In the fundamental WGM, the coupling between the amplitudes of the two interacting waves κ , satisfies equation (2-16) which is shown in **Figure 4-3** as a function of k and a . When the radius of the sphere changes, the pattern indicating optimal conditions for SHG bends (cf. **Figure 4-3**).

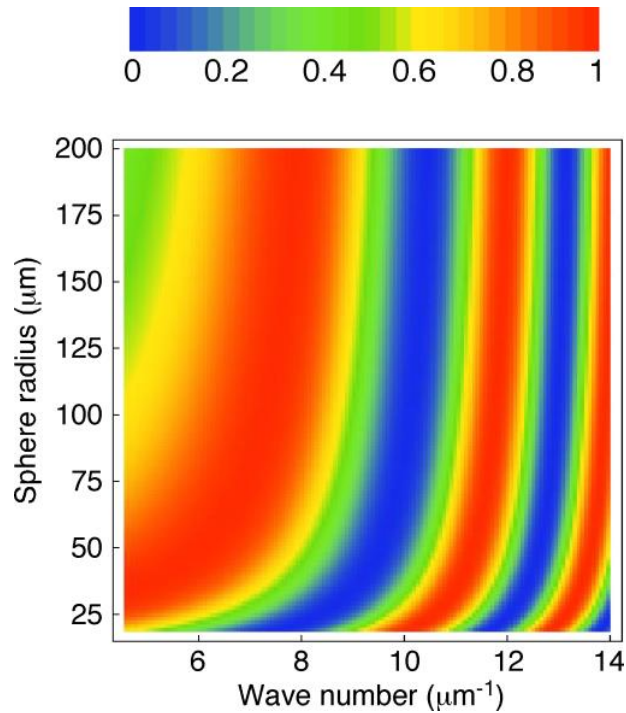


Figure 4-3. Equation (2-16) as a function of the radius of the sphere and wavenumber for the fundamental wave in vacuum. The arc length is fixed to $8.8 \mu m$ at the equator.

A periodic pattern of domains of width ℓ_c , which expression is given in Eq. (2-16), can be inscribed with 50 nm accuracy using an electron beam as discussed in Chapter 3. If the pattern of stripes on the sphere surface were to be projected on an equatorial plane perpendicular to the radius that passes through the center of the central stripe, one would obtain a pattern as the one shown in white in **Figure 4-4**. We wrote a periodical pattern on roughly one quarter of the sphere around the equator perpendicular to the stem that

holds it, as shown in **Figure 4-4**. The pattern consists of alternated stripes whose width must be exactly one coherence length of the corresponding nonlinear interaction.

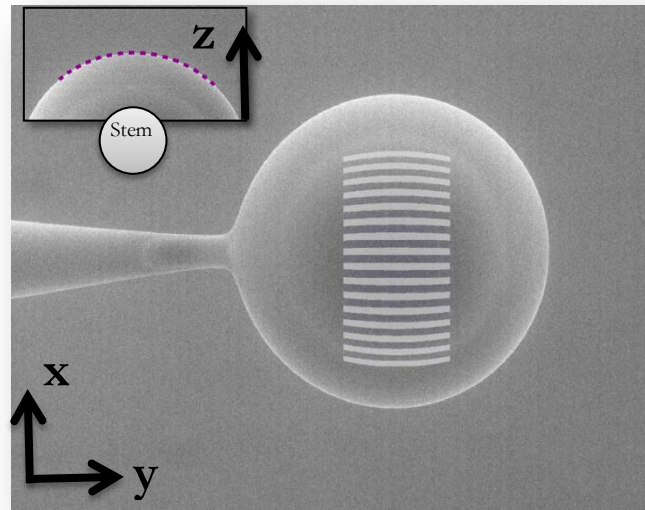


Figure 4-4. SEM image of the microsphere used in the experiment. The periodical pattern drawn on the sphere is superimposed on the SEM image of the sphere at the same scale. The diameter of the sphere was $359\mu\text{m}$. Inset: Change in z direction perpendicular to the e-beam.

The coordinates of such projections were introduced into the SEM control unit to define the xy motion of the sphere assuming that the xy plane is perpendicular to the e-beam. As long as the e-beam width remained constant, such xy motion produced on the sphere surface the desired pattern of stripes of equal length and width.

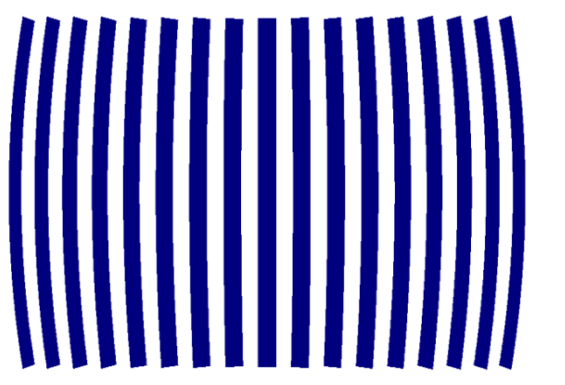


Figure 4-5. Pattern preparation at the electron beam lithography with a periodic pattern of domains of width ℓ_c as given in equation (2-16).

To compensate for e-beam divergence, we also moved the sphere in the z direction to ensure that the surface of the sphere always remained in focus with the e-beam, as the picture shown in the inset of **Figure 4-4**. Note that the pattern drawn did not reach the poles (c.f **Figure 4-5**), because the interaction region for fundamental WGM is mostly confined around the equatorial plane. Drawing the pattern up to the poles would have no positive effect and would only increase the manipulation of the sphere resonator, which in the end would result in a reduction of the Q factor.

Surface SHG in the WGM

To measure SHG we used a tunable modelocked Ti:Sapphire laser amplifier thermally stabilized emitting a 1kHz train of 150fs infrared pulses centered at 800nm in wavelength [Modelocked Ti:Sapphire laser “Mira” and Ultrafast amplifier “Legend” of Coherent Inc.]. An average power of $200\ \mu\text{W}$ of the train of pulses was coupled into an SMF-28 optical fiber. After travelling through the 1.5-m fiber used in the set-up, drawn schematically in **Figure 4-6.**, the pulses were lengthened to $\sim 1.1\text{ps}$. The fiber was

tapered, and at the center of such a tapered region, the diameter reached a minimum value around $\sim 1 \mu\text{m}$. By bringing the sphere close to the center of the tapered section, the light pulses were coupled into some of the fundamental WGM of the microsphere (45) (56). The radii of the majority of the spheres used in the experiments reported ranged from 177 to $183 \mu\text{m}$. Directly from the spherical harmonics, corresponding to the fundamental beam, we could determine the arc length of the fundamental field distribution inside the sphere to be close to $7.5 \mu\text{m}$. This coincides very well with the experimentally measured one from the picture shown in the inset of **Figure 4-6**. The generated second harmonic pulses at around 400 nm leaked out of the sphere because of Rayleigh scattering by defects on the sphere surface, and that light, after proper filtering, was detected using a reverse-biased photomultiplier tube (PMT). As seen in **Figure 4-6**, to maximize the collection of the scattered light, we used a microscope objective with numerical aperture 0.65.—The first step to optimize the conversion efficiency in each experiment was to move the sphere along the taper, while SHG intensity was measured as a function of such a sphere position. By simultaneously measuring the transmission through the fiber and the SHG intensity, we observed that as the transmission diminished, indicating a more effective coupling of the fundamental field from the fiber to the sphere, the observed SH intensity increased. Maximum SHG thus corresponded to minimum transmission through the fiber.

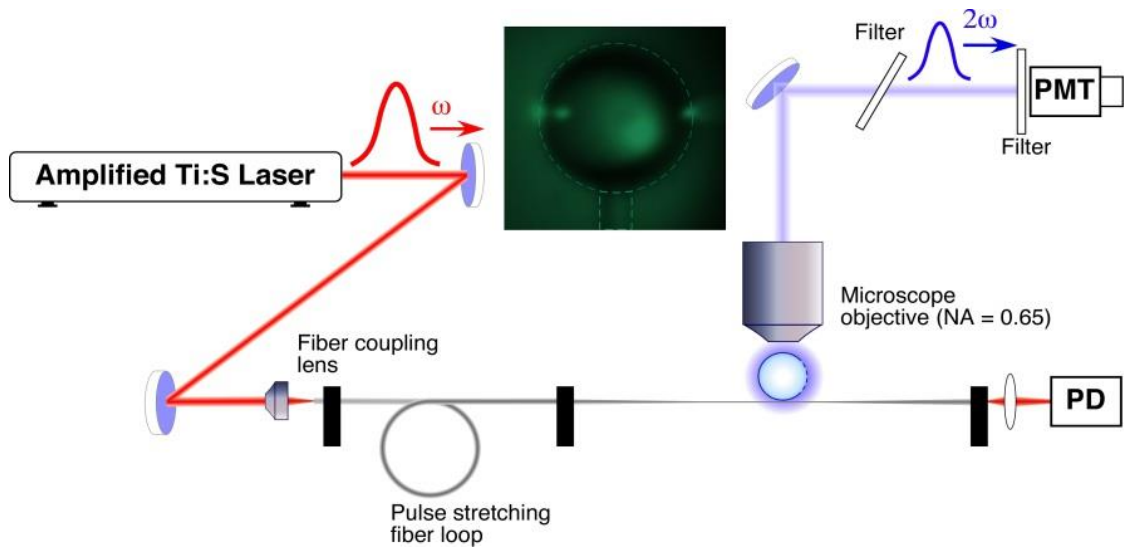


Figure 4-6. Schematic view of the experimental set-up used for measuring the SH light generated by the nonlinear grating at the surface of the microsphere. The fiber loop is used only in the experiments where the fundamental pulse is stretched to uniformly cover the entire perimeter of the sphere. The inset shows the polar and radial distribution of the WGM when the pulse is coupled into the microsphere (bright spot on the right). The picture was taken for a sphere doped with Erbium atoms to facilitate the visibility of the WGM. The other two spots on the left correspond to images or parasitic reflections formed by the sphere of the residual light uncoupled from the taper to the sphere.

The spheres we used in these experiments were coated from solutions of CV which concentration ranged from 2.5×10^{-4} to 1.5×10^{-9} Molar. At concentrations above 2.5×10^{-5} Molar, the Rayleigh-scattered SH light from the sphere surface was detectable using the set-up described above. As shown by the red dots of **Figure 4-7** by tuning the wavelength in a range between 790 nm and 820 nm , SHG strongly peaks at exactly 403 nm very close to the quasi-phase matching condition at 403.5 nm predicted using equation (2-16). from the theory in (25). In this numerical application of the theory developed in chapter 2, we used no adjustable parameters and all the numbers used correspond to the actual parameters of the experiment or materials. The agreement is

remarkable and the 0.5 nm displacement could be attributed to the slight shift in the resonances predicted by the analytical model or a small error in measuring the diameter of the sphere. Note that as indicated in chapter 2 quasi-phase matching ensures that both waves propagate in resonant modes of the cavity. As indicated, the light at the fundamental or second harmonic frequencies travels in more than one resonant mode of the cavity and consequently conservation of energy is ensured within the bandwidth of the pulses used which is approximately 5 THz. Using a sphere with a $Q = 8.9 \times 10^6$ coated with a 2.5×10^{-5} M solution of CV we confirmed that the SHG dependence with the fundamental pumping intensity is quadratic. Indeed, we placed an NG5 filter that provides a 50% transmission at, both, 400nm and 800nm, first at the entrance of the coupling fiber and afterwards in front of the PMT. In the first measurement the SHG is reduced close to 25% while in the last one is only reduced to 50% confirming the quadratic behavior of the SHG when using the spherical micro-resonator configuration described above.

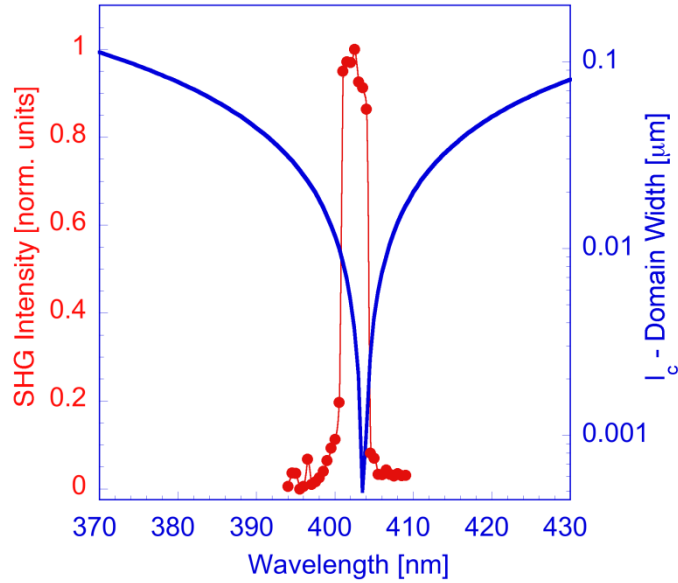


Figure 4-7. Second harmonic generation as a function of half the wavelength of the fundamental wave (red dots) when the coating solution was $2.5 \times 10^{-4} \text{ M}$. Experimental domain width minus the calculated coherence length at the equator as a function of half the wavelength of the fundamental wave in a logarithmic scale (blue solid line). The lines are only a guide for the eye.

The role played by the phase matching mechanism was further confirmed by tuning the fundamental wavelength using an optical parametric oscillator (OPO) to shift the fundamental wavelength to around 900 nm . In that case, the radius of the sphere was $124 \mu\text{m}$ and the grating pitch close to $10.2 \mu\text{m}$. As seen in **Figure 4-8** the phase matching peak obtained was broader than with the original laser-pumped sphere. This was due to the OPO output, which is broadened by 27 nm relative to the original laser pulse.

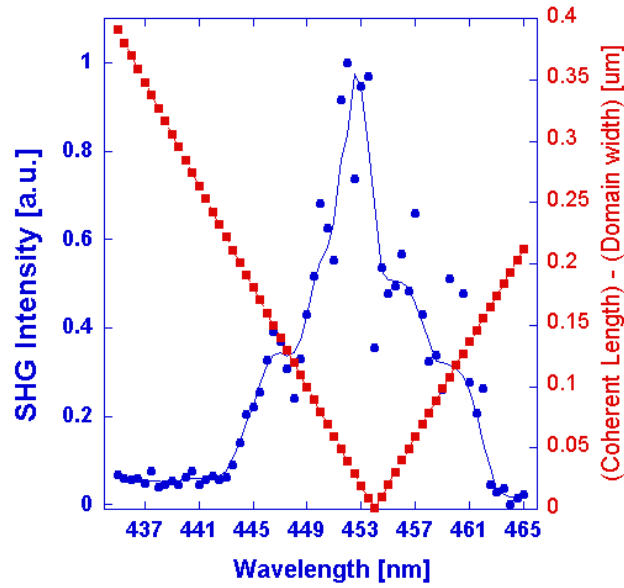


Figure 4-8. SHG as a function of half the wavelength of the fundamental wave when the pump wavelength is centered at 900 nm [$2.5 \times 10^{-4}M$]. The red dotted lines indicate the wavelength for the quasi-phase matching condition calculated using an analytical approximate expression (2-16) minus the experimental domain width. The lines are only a guide for the eye.

Temporal Walk-off Compensation between Fundamental and SH Pulses

When the Q of the spheres used above ranged from 3.3×10^6 up to 6.9×10^7 in the conditions described above no SH signal could be detected for concentrations below 2.5×10^{-5} M. Temporal walk-off between fundamental and SH pulses reduced the interacting length down to a very short distance, equivalent to having a Q factor of approximately 10^4 . To take full advantage of the nominal Q factor, we stretched the pulses to a length equal or larger than the perimeter of the spheres used. We used 140 meters of an optical fiber loop placed in between the entrance of the fiber and the tapered region, as schematically shown in **Figure 4-6**. When the pulsed reached the coupling region between the fiber and the sphere it stretched up to approximately ~ 100 ps, which was close to 21

times the perimeter of the largest sphere used in the experiments reported. The combined effect of pulse stretching and walk-off in the fiber improved the signal detection efficiency by four to five orders of magnitude.

To achieve an optimal pulse walk-off we tested four different fiber lengths. The results obtained are summarized in Table 2. In all four cases the SH signal was monitored while scanning the wavelength of the input laser within the 100 nm range of tunability of the amplified laser system used. The CV coating concentration used was $1 \times 10^{-8} M$ while the sphere Q factor was 3.82×10^7 . For the 1.5 m fiber, the pulse intensity remained the largest one, 12.2 % relative to the intensity of the original non-stretched pulse. However, no phase matching peak could be observed because the SH signal from the molecules was overlapped with the white light generated at the pulse entrance tip of the fiber, combined with the fact that a pulse length shorter than the perimeter of the micro-resonator cavity prevented pulse walk-off compensation. When the pulse was stretch up to 10,7 ps, corresponding to close to two times the pulse roundtrip time within the resonator, we still did not observe any phase matching peak. In that case the delay between the fundamental pulse and white light was only 1.58 ns.

Table 2. SHG performance for four different lengths of the pulse stretching fiber loop.

SHG performance for four different lengths of the pulse stretching fiber loop				
Fiber length (m)	1.5	+10	+140	+400
SH peak (arb. units)	No PM† peak	No PM peak	2.246	No PM peak
Pulse FWHM (ps)	1.1	10.7	102.9	291.9
Peak Intensity FF*(%)	12.2	1.3	0.13	0.046
Delay‡ (ns)	0.24	1.58	22.17	63.33

One single sphere was used in all the measurements with: $Q = 3.82 \times 10^7$, $R = 179 \mu\text{m}$, and a CV coating concentration = $1 \times 10^{-8} M$.

The first two rows correspond to experimentally measured values. The first two columns of the third row are the result of an autocorrelation measurement. The last two columns of the third row are determined using the pulse width increase given in (44). The fourth row is calculated using the values measured in the previous rows. The fifth row is determined from the group velocity dispersion in fused silica fibers.

†PM indicates phase matching.

*Corresponds to the peak intensity of fundamental field at the taper portion of the fiber relative to the peak intensity of the incident non-stretched pulse.

‡Corresponds to the delay between the fundamental pulse and the portion around 400 nm of white light generated at the entrance tip of the fiber.

Proper temporal filtering from the white light was not possible provided the large Q resulted in a signal lifetime close to 7 ns. Using a 140 m fiber we introduced a delay time equivalent to 22.2 ns between the fundamental and white light pulses. Such delay was sufficient to temporally separate the SH signal from such white light. A proper separation requires a delay about 3 times the decay time of the SH signal which in the majority of measurements we performed ranged between 6 to 8 ns. In addition, the pumping pulse was stretched close to 20 times the equator length and walk-off could be perfectly compensated. Further improving of the sensitivity could be reached by slightly increasing the intensity of the laser input pulse as indicated above in the main text. Additional stretching of the pulse to reach a larger delay which would be needed if very large Q factor spheres were to be used, proved to be unsuccessful. The failure in measuring a phase matching SH peak could be attributed to a 0.046% reduction in peak intensity at the tapered region. In summary, the 140 m fiber length proved to be an optimal one which also allowed us to test spheres with Q factors slightly larger.

SHG and Sphere Q-factor

Combining the quasi-phase matching configuration with the pulse stretching discussed above, we were able largely reduced the molecular density needed to obtain a measurable SH signal. When performing such high-sensitivity measurements using CV solutions at concentrations equal or below $5 \times 10^{-9}\text{M}$, one has to find a trade-off between a high level of pumping intensity to increase the efficiency of the SHG from CV, and a lower pumping level to prevent the onset of other unwanted nonlinear processes, such as white light generation at the tapered portion of the fiber or light induced damaging of the fiber entrance tip. This left a window for the pump-power level, which narrowed down as the

molecular surface concentration was decreased. For the lowest molecular concentration that we measured, the optimal pump energy corresponded to ~ 0.025 nJ per pulse.

Prior to measuring SH with the lowest concentration possible, one must evaluate in detail the role that the Q factor had in the efficiency of the SHG process by comparing the SH intensity when two different spheres with different Q factors were used as micro-resonators. It is important to note that the experimental conditions for the two experiments were kept exactly the same. As may be seen in **Figure 4-9**, a comparison of the integrated SH intensity over time indicates that a 4.9 times increase in the Q factor resulted in an increase in the energy conversion by a factor of 25, slightly larger than Q^2 .

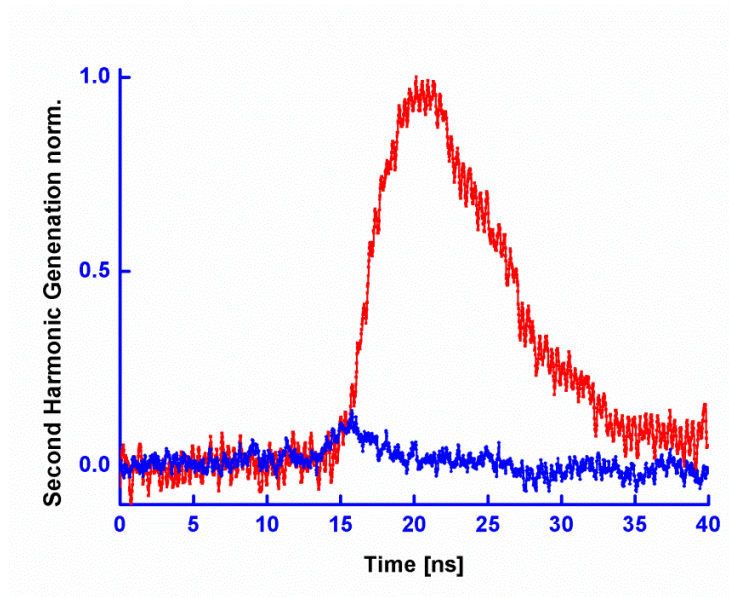


Figure 4-9. SH intensity as a function of time, using a sphere with $Q = 1.83 \times 10^7$ (red solid line) and a sphere with $Q = 3.72 \times 10^6$ (blue solid line). Both spheres were coated with a 5×10^{-7} M solution of CV and periodically patterned to achieve the phase-matching condition. All the parameters of the experimental setup, coupling taper, input intensity and so on were kept equal. The difference in Q factor must be attributed mostly to a difference in the eccentricity, whereas the difference in radius between the two spheres was only 16% one in the vertical scale corresponds to an intensity current of $96 \mu\text{A}$.

This clearly demonstrated the positive effect brought to the nonlinear interaction by the light localization within the micro-resonator. The build-up of intensity at the SH frequency is dramatically more effective when the Q is larger. In other words, as one would have expected there is an increase in the total dwell time for the SH light pulse but, there is also an increase, larger than 7 times, for the maximum SH intensity measured shown in **Figure 4-9**. Using a new pair of micro-spheres, we repeated the experiment but reducing the CV coating concentration molarity by a factor of 100. We observed that a 3.6 times increase in the Q factor lead to a 19.1 times increase in the SH energy conversion, again less than Q^3 but larger than Q^2 . This confirmed the relevant role played by the Q factor. Using the coupled mode approach we determined analytically the role played by the sphere Q factor on the SHG. Using the same notation as in chapter 2, with the appropriate choice of units,

$$\left(\frac{\omega}{Q_1}\right)|\alpha_1|^2 \tag{4-1}$$

is the power lost by the fundamental mode by linear processes, where Q_1 is the associated quality factor. Besides the natural far field radiation of WGM from perfect spheres, decay channels include Rayleigh scattering from surface imperfections, parasitic absorption, or out-coupling to neighboring waveguides. Similarly,

$$\left(\frac{2\omega}{Q_2}\right)|\alpha_2|^2 \tag{4-2}$$

is the power lost by the second harmonic mode where Q_2 is the associated quality factor. A fraction of this power is collected as a usable signal. Given the optical power P_{taper} in the taper fiber and an out-coupling quality factor Q_0 , energy is injected in the fundamental mode at a rate of $\frac{P_{taper}}{Q_0}$ at resonance. Equilibrium is thus reached when

$$\left(\frac{\omega}{Q_1}\right) |\alpha_1|^2 = \frac{P_{taper}}{Q_0} \quad (4-3)$$

On the other hand, standard couple-mode theory dictates that

$$\left(\frac{\omega}{Q_2} + i\Delta\omega\right) \alpha_2 = i\kappa |\alpha_1|^2 \quad (4-4)$$

Therefore, the out-coupled SHG intensity is proportional to

$$(2\omega/Q_2) |\alpha_2|^2 = \frac{2|\kappa|^2 (Q_1^2 Q_2 / Q_0^2)}{\omega^3 (1 + \Delta\omega^2 Q_2^2 / \omega^2)} P_{taper}^2 \quad (4-5)$$

Hence, when energy is conserved $\Delta\omega = 0$, and assuming that $Q_1 = Q_2 = Q$, we expect the SHG signal to scale as Q^3 in the optimal conditions. The fact that experimentally we measure a proportionality below Q^3 may be attributed to small variations in the coupling conditions when different spheres are used that eventually results in a change in the Q_0 factor.

SHG and Molecular Density

To study the sensitivity of SH signal to CV concentration, we performed a set of experiments to determine the SHG dependence on the concentration of molecules using four different CV concentration solutions ranging from 5×10^{-9} up to 5×10^{-6} . To avoid dispersion in the diameter or Q factors, we performed the experiment using only one sphere that we coated starting by the smallest concentration and writing the grating and then performing the SH measurement. Subsequently, we repeated this procedure 3 times, each time with a concentration that was 10 times larger than the previous one. As shown in **Figure 4-10**, the SH signal increases with increasing concentration with a growth rate that deviates from the quadratic growth rate one would expect.

It is not clear what the origin of the SHG efficiency saturation is as the CV concentration increases. One possibility could be a small degradation in the Q factor after the coating procedure is repeated each time. For instance, we observed a 20% decrease of the Q when the sphere was coated with a $5 \times 10^{-7} M$ solution of CV. Molecular absorption alone, however, cannot account for the slow growth rate observed in **Figure 4-10**. Possibly, another less controllable source that lowers the Q factor each time a new grating is inscribed may also exist. Another source of discrepancy could arise from a degradation of the quasi-phase matching condition caused by the residual molecules left from the previous coating leading to a more shallow grating.

We also measured SH from a similar sequence where we did not perform the grating in any of the steps. As seen in **Figure 4-10**, the SH signal measured was in those cases down to noise level. This shows that in detection devices based on the results reported, it would be

very simple to discriminate the molecule to be detected from any other molecule that could attach to the surface even if such unwanted molecule is a better SH generator. Following a patterned functionalization only the molecule to be detected would end up in the periodic pattern required for quasi-phase matching. However, provided that no other change is introduced except for a change in the number of molecules, the proportionality relation $I_{2\omega} \propto N^2$, N being the number of molecules, must hold, as in the UV flashlamp experiments reported below where nothing in the experimental set-up was modified during the course of the experiment.

We also measured SH from a similar sequence where we did not perform the grating in any of the steps. As seen in **Figure 4-10**, the SH signal measured was in those cases down to noise level at all concentrations. This shows that in detection devices based on the results reported, it would be very simple to discriminate the molecule to be detected from any other molecule that could attach to the surface even if such unwanted molecule is a better SH generator. Following a patterned functionalization only the molecule to be detected would end up in the periodic pattern required for quasi-phase matching.

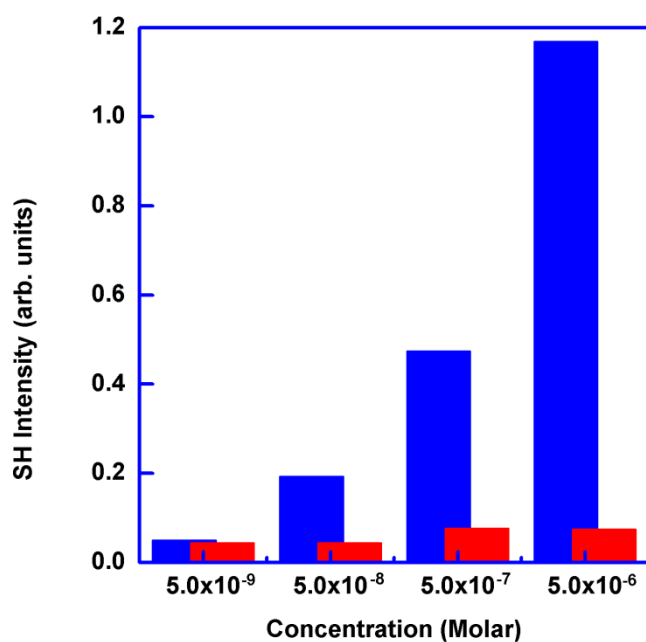


Figure 4-10. Second harmonic signal in arbitrary units for four different surface concentration of nonlinear molecules when a grating was written (blue bars) and when no grating was written (red bars). In the horizontal axis we indicate the concentration of the original solution used to prepare the monolayers.

SHG from the smallest Number of Molecules

To determine the absolute sensitivity of the surface SHG in the microspheres reported in the current thesis, we performed an experiment to estimate what was the minimum number of molecules required to measure a change in the SH signal. We measured the SH signal decrease produced when subsequent 1 sec UV flashes from a disinfection UV lamp with an intensity peak at 253.7 nm were shone on the sphere to photodegrade the CV. We considered two different spheres coated with two different concentrations.

To estimate the total number of molecules participating in the interaction before such UV molecular degradation experiment began, we had to consider the total number of coated stripes on the sphere surface and the interaction area within each stripe. Such area was equal to the product of the equatorial length of the stripe times the interaction length in the polar direction. To determine such length in the polar direction we used Equation (2-16) Let's assume that for the fundamental and SH waves in the WGM, which are concentrated on the equator, we have $M = L$, $m = l$, , and

$$Y_{LM} \propto e^{-L(\pi/2-\theta)^2/2} \quad (4-6)$$

$$Y_{lm} \propto e^{-l(\pi/2-\theta)^2/2} \quad (4-7)$$

Provided that any of the nonzero components of the nonlinear susceptibility $\chi^{(2)}$ proportional to the surface density of molecules $\rho(\theta, \varphi)$, Equation (2-10) becomes

$$\kappa = \iint \rho(\theta, \varphi) e^{-(L+2l)(\pi/2-\theta)^2/2} \sin \theta d\theta d\varphi. \quad (4-8)$$

The integrand above leads to an effective density which is halved when

$$|\pi/2 - \theta| > \left(\frac{2 * \ln(2)}{L + 2l} \right)^{1/2} \quad (4-9)$$

On the other hand, $L \sim 2n_{s2}ka = 4\pi n_{s2}a/\lambda$, $l \sim n_{s1}ka = 2\pi n_{s1}a/\lambda$ where λ is the fundamental wavelength. The effective arc length in the θ direction is, therefore:

$$s = 2a \times \left(\frac{2 * \ln(2)}{L + 2l} \right)^{1/2} = \left(\frac{2 * \ln(2) * a\lambda}{\pi(n_{s2} + n_{s1})} \right)^{1/2} \quad (4-10)$$

Assuming $a=177\mu m$, $\lambda = 800nm$, $n_{s1} = 1.45$ and $n_{s2} = 1.47$, this yields $s=4.6\mu m$. Provided that CV density on the surface sphere at the $(1.55 \pm 0.04) \times 10^{-9}M$ concentration was $(7.90 \pm 0.14) \times 10^7$ molecules per cm^2 the length of the strip at the equator in the azimuthal direction is equal to $8.7\mu m$ and the total number of stripes in the sphere used was 16, in the SH measurements shown in **Figure 4-4** the total number of molecules participating in the interaction at the starting point, before any UV flash was shone, was approximately $\sim 506 \mp 9$.

After shining a ultraviolet flash lasting for a time δt , the number of molecules on the surface decreases as

$$\delta \aleph = -\aleph \check{\alpha} I_{UV} \delta t \quad (4-11)$$

where \aleph is the number of molecules, I_{UV} is the ultraviolet intensity at the sphere surface and $\check{\alpha}$ is a constant of proportionality to maintain the units correct. After integration with respect to time, the number of molecules is given by

$$\aleph = \aleph_0 e^{-\check{\alpha}'t} \quad (4-12)$$

where \aleph_0 is the initial number of molecules and $\check{\alpha}' = \check{\alpha}I_{UV}$. By using equation (4-12) and the direct proportionality of the intensity of the SHG light to the square of the number of molecules, the measured SH intensity at a given time may be written as:

$$I_{2\omega} = \check{\beta}I_{\omega}^2 \aleph^2 + I_{BG} \quad (4-13)$$

where I_{BG} is the background signal noise at the SH frequency not coming from the molecules, $\check{\beta}$ is a constant and I_{ω} is the fundamental pump intensity. If we normalize such a measured SH intensity to the intensity of the incident fundamental field, then the following linear relation must hold

$$\frac{I_{2\omega}}{I_{\omega}} = \check{\beta}I_{\omega} \aleph^2 + \frac{I_F}{I_{\omega}} \quad (4-14)$$

$$\frac{I_{2\omega} - I_F}{I_{\omega}} = \check{\beta}I_{\omega} (\aleph_0 e^{-\check{\alpha}t})^2 \quad (4-15)$$

$$\sqrt{\frac{I_{2\omega} - I_F}{I_{\omega}}} = \sqrt{\check{\beta}I_{\omega}} \aleph_0 e^{-\check{\alpha}t} \quad (4-16)$$

$$\ln\left(\sqrt{\frac{I_{2\omega} - I_F}{I_\omega}}\right) = -\check{\alpha}t + \ln\left(\sqrt{\check{\beta}I_\omega N_0^2}\right) \quad (4-17)$$

The experimental values for the left hand side of equation (4-17) are plotted as a function of the ultraviolet flash number in (4-16). The value of $\check{\alpha}'$ is extracted from the slope and used in equation (4-17) to estimate the number of molecules remaining after each ultraviolet flash is shone. As shown in **Figure 4-11**, after the first UV flash the total number of molecules available for SHG goes down to $(506-323)=183$, after the second to $(323-206)=117$, and after the third one to $(206-131)=75$. This indicates that approximately between 50-100 molecules are needed to detect a measurable change in SHG. After the third flash the signal is already down to the noise level.

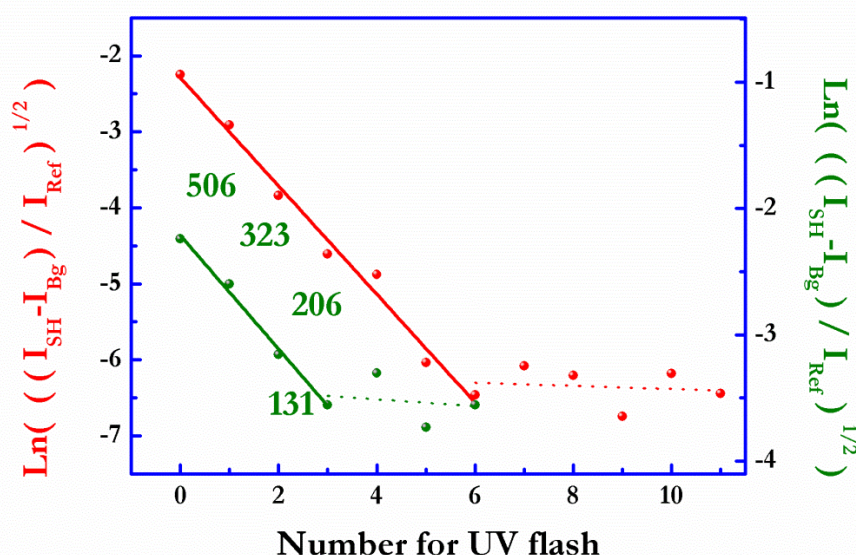


Figure 4-11. Natural logarithm of the measured SH intensity decrease produced when subsequent 1 sec UV flashes (horizontal axis) were shone on the sphere to photodegrade the CV. The background noise is subtracted from the measured intensity and then such difference divided by the reference input intensity to ensure a unitless logarithm argument and proportionality to the molecular surface density. Two different

spheres were coated with a $1.55 \times 10^{-9} M$ solution of CV (green dots) and with a $1 \times 10^{-7} M$ solution of CV (red dots). The numbers by the green dots should not be taken literally and are only indicative of the molecules that participate in the SHG prior to the shining of each UV flash. The solid lines indicate a linear adjustment to the portion of data that shows a decrease while the dotted lines indicate a linear adjustment to the almost flat portion of the data.

Similarly, we can determine the sensitivity when the sphere is coated with a 10^{-7} concentration of molecules. As seen in **Figure 4-11**, the square root of the SH intensity displayed in both cases a similar behavior. One sees a relatively fast exponential decay followed by an almost constant signal which is down to the noise level. Since the square root of the SH intensity is proportional to the number of molecules on the surface, and such number decreases exponentially with the UV exposure time, we can accurately estimate the number of molecules required to see a measurable change in SHG.

Conclusion

With spherical microresonator configuration studied in this chapter to obtain a measurable SH signal one needs a molecular surface density $\sim 10,000$ times lower than when SHG is measured directly from a flat surface under similar pumping conditions. The role of the cavity in the resonator case is clearly confirmed when the enhancement ratio provided by the resonator was measured to scale between Q^2 and Q^3 . When we consider the total number of molecules, to obtain a measurable signal, one needs at least 4×10^6 molecules in the flat-surface configuration, as opposed to 50–100 for the resonator case, in which the molecules only detect the evanescent tail of the field stored in the microresonator. Note that, for the flat-surface configuration, a high pumping intensity directly hitting the molecules causes a rapid degradation, which does not occur in the resonator case. Earlier configurations based on microresonators to detect single objects could not be used to detect small molecules, even if a large number were to be used. Such configurations are based on producing a local change on the surface of the microresonator, and this is only possible if one uses large molecules or tens of nanometre-sized particles. The particular setup of the configuration we studied in the current thesis, in which molecules assemble at an interface at which the interaction is enhanced by the large Q factors available, opens up the possibility to obtain an efficient SHG from any type of molecules, even if they are centrosymmetric or if the dipole moment in the ground state is zero, as for the molecule used. In other words, any kind of label-free, large or small molecule is, in principle, detectable.

Conclusion and Outlook

In the current thesis work we have demonstrated experimentally that the nonlinear activity of organic molecules deposited on a spherical surface could be erased using an electron beam, which allowed us to write the exact periodic pattern needed for quasi-phase matched surface second harmonic. The periodic quasi-phase-matched SHG implemented in the current thesis has the added value that contributions from the bulk or the non-patterned interface are essentially negligible, as they are, in general, not phase matched unless some very particular requirements for the set of parameters that define the microresonator are met. We have also shown that SHG in the microresonator configuration considered provides a means for temporal walk-off compensation when the interacting pulses are longer than the resonator perimeter. The quasi-phase-matched SHG experimental demonstration reported is the first step to many other parametric process and opens up the possibility to study experimentally phase-matched quadratic NL optics in any circular high-

Q cavity configuration that remained, until recently, very much unexplored. SHG in the configuration studied in this thesis may prove to be very effective as a sensing mechanism.

A versatile sensing device must be capable of detecting label-free or unmarked objects, exhibit a high sensitivity, and be able to distinguish positive signals coming from the object to be detected from signals triggered by other unwanted objects present in the environment of the device. Label-free detection can be achieved when the property on which the sensing device is based is shared by many different types of objects. As is well known, generation of light via a quadratic nonlinear process is rather universal since all forms of matter may be used, in principle, to generate SH.

To reach large sensitivities, in some optical devices one may take advantage of the optical cavity configuration considered that would allow for the light to interact elastically many times with the object to be detected. The number of interactions is simply given by the ratio of the photon cavity lifetime to the round-trip time, which can be computed as

$$\frac{Q\Delta\nu_{fsr}}{2\pi\nu} \tag{0-1}$$

where $\Delta\nu_{fsr}$ is the free-spectral range and ν is the frequency (in Hz). This is, essentially, the cavity finesse. Such a number becomes close to one million when microsphere resonators with Q factors of 10^8 – 10^9 are used.

At the moment, in terms of concentration, resonance shift-based systems present a clear advantage, while SHG-based ones are more suitable for the detection of extremely small

objects. The quasi-phase matching mechanism required to obtain effective SHG provides in itself the means to avoid the detection of unwanted objects. To sense a specific type of molecule by SHG using microsphere resonators, one would have to cover them with a monolayer surface of molecular sites where the specific molecule to be detected would bind. To obtain enhanced quasi-phase matched SHG, one would have to previously periodically pattern such a monolayer of sites. This could be performed using an electron beam periodic patterning similar to that implemented in in this thesis. In such a way, molecules would bind more effectively to the proper stripes on the sphere surface and quasi-phase matching would be possible. Note that, even in the case where single-molecule detection is considered, the same periodic patterning is necessary.

Note that, except for very specific radii and conditions, the contribution from the resonator surface would not be phase matched. Such a contribution could not grow even if the value of Q were high. There are, still, many issues to be resolved before SHG in WGMs can be effectively used in very sensitive sensing.

For instance, work must be done on reducing the area aspect ratio between the sensitive part of the sphere surface and the one that does not contribute to sensing. A possible path to markedly reduce the molecular concentration needed for detection might be by forming arrays of spheres, which would be coupled to each other in order to enhance the sensitivity to concentration, forming what could be named an optical nose.

We see, however, that the work performed over the last years in the field of SHG in circular geometries and WGMs in ring or spherical micro-resonators has laid the foundations for the development of such new types of sensing devices with unsurpassed detection sensitivity. Finally, the interest in nonlinear optics in ring or spherical micro-

resonators is not limited to sensing. Fundamental aspects of physics, such as quantum state entanglement or cavity-enhanced nonlinear interactions, are still to be considered in such circular geometries.

Bibliography

1. *Optical Resonators with Whispering-Gallery Modes-Part II: Applications.* **Matsko, V. S. Ilchenko and A. B.** 15, 2006, IEEE J. Sel. Top. Quantum Electron., Vol. 12.
2. *Optical Microcavities.* **Vahala, K. J.** 839, 2003, Nature , Vol. 424.
3. *Optical Resonators with Whispering-Gallery Modes-Part I: Basics.* **A.B. Matsko and V.S.Ilchenko.** 3, 2006, IEEE J. Sel. Top. Quantum Electron., Vol. 12.
4. *Protein Detection by Optical Shift of a Resonant Microcavity.* . **Vollmer F., Braun D., Libchaber A., Khoshima M., Teraoka I., Arnold S.** 2002, Appl. Phys. Lett. , Vol. 80, pp. 4057-4059.
5. *Shift of Whispering-Gallery Modes in Microspheres by Protein Adsorption.* . **Arnold S., Khoshima M., Teraoka I., Holler S., Vollmer F.** 2003, Opt. Lett. , Vol. 28 , pp. 272-274 .
6. *Refractometric Sensors Based on Microsphere Resonators.* **Hanumegowda N. M., Stica C. J., Patel B. C., White I., and Fan X.** 2005, Appl. Phys. Lett., Vol. 87, p. 201107 .
7. *Photoinduced Transformations in Bacteriorhodopsin Membrane Monitored with Optical Microcavities.* **F. Vollmer, Topolancik J.** 2007, Biophysical Journal, Vol. 92, pp. 2223–2229.

8. *Single Virus Detection From the Reactive Shift of a Whispering-Gallery Mode.* **F. Vollmer, S. Arnold, D. Keng.** 52, 2008, PNAS, Vol. 105, pp. 20701-20704.
9. *Nano-sensing With A Reference Interferometer.* **T. Lu C, H. Lee, T. Chen, S. Herchak, J-H Kim, and K. Vahala.** 2010, Conference Paper Frontiers in Optics Rochester.
10. *Detecting Single Viruses and Nanoparticles Using Whispering Gallery Microlasers.* **He, Lina et. al.** 7, s.l. : Nature Nanotech, 2011, Vol. 6, pp. 428-432.
11. *Whispering-Gallery-Mode Biosensing: Label-Free Detection Down to Single Molecules.* **F. Vollmer & S. Arnold.** 2008, Nature Methods, Vol. 5, pp. 591 - 596.
12. *Whispering Gallery Mode Biosensor for Label-Free Detection of Single Molecules: Thermo-Optic vs. Reactive Mechanism.* **S. Arnold, S. I. Shopova, and S. Holler.** 1, 2010, Optics Express, Vol. 18, pp. 281-287.
13. *On-Chip Single Nanoparticle Detection and Sizing by Mode Splitting in an Ultrahigh-Q Microresonator.* **Zhu J., Ozdemir S. K., Xiao Y.F., Li L., He L., Chen D.R., Yang L.** 1, 2009, Nature Photonics, Vol. 4, pp. 46-49.
14. *Split Frequency Sensing Methods and Systems.* **Lu T., Su, Tsu-te J. Vahala K. J. Fraser S. E.** 2010, United States Patent , Vol. 20100085573.
15. *Cavity quantum electrodynamic enhancement of stimulated emission in microdroplets.* **Campillo A.J., Eversole J.D. and Lin H-B.** 1991, Phys. Rev. Lett., Vol. 67, pp. 437-440.

16. *Ultralow-Threshold Raman Laser Using a Spherical Dielectric Microcavity.* **S. M. Spillane, T. J. Kippenberg and K. J. Vahala.** 2002, *Nature*, Vol. 415, pp. 621-623.
17. *Ultra-Low-Threshold Erbium-Implanted Toroidal Microlaser on Silicon.* **A. Polman, B. Min, J. Kalkman, T. J. Kippenberg and K. J. Vahala.** 2004, *Appl. Phys. Lett.*, Vol. 84.
18. *Kerr-Nonlinearity Optical Parametric Oscillation in an Ultrahigh-Q Toroid Microcavity.* **T. J. Kippenberg, S. M. Spillane, and K. J. Vahala.** 8, 2004, *Phys. Rev. Lett.*, Vol. 93, p. 083904.
19. *Parametric Oscillations in a Whispering Gallery Resonator.* **A. A. Savchenkov, A. B. Matsko, M. Mohageg, D. V. Strekalov, and L. Maleki.** 2, 2007, *Opt. Lett.*, Vol. 32.
20. *Label-Free Detection with High-Q Microcavities: A Review of Biosensing Mechanisms for Integrated Devices.* **F. Vollmer, L. Yang.** 2012, *Nanophotonics*, Vol. 1, pp. 267–291.
21. *Quasi-Phase-Matched Second Harmonic Generation: Tuning and Tolerances.* **M. M. Fejer, G. A. Magel, D. H. Jundt, and R. L. Byer.** 11, s.l. : *IEEE Journal of Quantum Electronics*, 1992, Vol. 28, pp. 2631-2654.
22. *Low-Threshold Parametric Nonlinear Optics With Quasi-Phase-Matched Whispering-Gallery Modes.* **V. S. Ilchenko, A. B. Matsko, A. A. Savchenkov, and L. Maleki.** 6, 2003, *JOSA B*, Vol. 20, pp. 1304-1308.
23. *Whispering-Gallery-Mode Analysis of Phase-Matched Doubly Resonant Second-Harmonic Generation.* **Féron, Y. Dumeige and P.** 063804, 2006, *Phys. Rev. A*, Vol. 74.

24. *Enhanced Second-Harmonic Generation in AlGaAs Microring Resonators.* **Z. Yang, P. Chak, A. D. Bristow, H. M. van Driel, R. Iyer, J. S. Aitchison, A. L. Smirl, and J. E. Sipe.** 2007, *Opt. Lett.*, Vol. 32, pp. 826-828.
25. *Whispering-Gallery-Mode Phase Matching for Surface Second-Order Nonlinear Optical Processes in Spherical Microresonators.* **G. Kozyreff, J. L. Dominguez Juárez, and Jordi Martorell.** 043817, 2008, *Phys. Rev. A*, Vol. 77.
26. *Naturally Phase-Matched Second-Harmonic Generation in a Whispering-Gallery-Mode Resonator.* **J. U. Fürst, D. V. Strekalov, D. Elser, M. Lassen, U. L. Andersen, C. Marquardt, and G. Leuchs.** 15, s.l. : *Phys. Rev. Lett.*, 2010, Vol. 104.
27. *Nonlinear Optics and Crystalline Whispering Gallery Mode Cavities.* **V.S. Ilchenko, A. A. Savchenkov, A. B. Matsko, and L. Maleki.** 4, 2004, *Phys. Rev. Lett.*, Vol. 92.
28. *Visible Continuous Emission from A Silica Microphonic Device by Third-Harmonic Generation.* **T. Carmon and K. J. Vahala.** 2007, *Nature Physics*, Vol. 3, pp. 430-435.
29. *Highly Tunable Low-Threshold Optical Parametric Oscillation in Radially Poled Whispering Gallery Resonators.* **T. Beckmann, H. Linnenbank, Steigerwald, B. Sturman, D. Haertle, K. Buse, I. Breunig.** 2011, *Phys. Rev. Lett.*, Vol. 106, pp. 143903-4.
30. *Second Order Parametric Processes in Nonlinear Silica Microspheres.* **Y. Xu, M. Han and A. Wang, Z Liu and J. R. Heflin.** 100, 2008, *Phys. Rev. Lett.*, Vol. 16, p. 163905.

31. *Blue-Pumped Whispering Gallery Optical Parametric Oscillator*. **C.S.Werner, T. Beckmann, K.Buse, I. Breunig**. 20, 2012, Opt. Lett., Vol. 37, pp. 4224-4226.
32. *Nonlinear Optics in Crystalline Whispering Gallery Resonators*. **C. Marquardt, D. Strekalov, J. Fürst, M. Förtsch, G. Leuchs**. 7, Optics & Photonics News, Vol. 24, pp. 38-45.
33. *High-Q UV Whispering Gallery Mode Resonators Made of Angle-Cut BBO Crystals*. **G. Lin, J. Fürst, D. Strekalov, I. S. Grudin, N Yu**. 19, 2012, OPTICS EXPRESS 21372, Vol. 20, pp. 21372-21378.
34. *Spherical Whispering Gallery Mode Microresonators*. **A. Chiasera, Y. Dumeige, P. Feron, M. Ferrari, Y. Jestin, G. Nunzi Conti, S. Pelli, S. Soria G. C. Righini**. 3, 2010, Laser & Photon. Rev., Vol. 4, pp. 457–482.
35. *Nonlinear Optics in Spheres: From Second Harmonic Scattering to Quasi-Phase Matched Generation in Whispering Gallery Modes*. **G. Kozyreff, J.L. Dominguez-Juarez, J. Martorell**. 6, s.l. : Laser Photonics Rev., 2011, Vol. 5, pp. 737-749.
36. *Fundamentals of Photonics*. **B.E.A. Saleh, M.C. Teich**. [ed.] Wiley & Sons. 2007.
37. *Cavity QED with High-Q Whispering Gallery Modes*. **D. W. Vernooy, A. Furusawa, N. Ph. Georgiades, V. S. Ilchenko, and H. J. Kimble**. 4, 1998, Phys. Rev. A, Vol. 57, pp. R2293- R2296.
38. *Microring Resonator Channel Dropping Filters*. **B. E. Little, S. T. Chu, H. A. Haus, J. Foresi, and J.-P. Laine**. 6, 1997, J of Lightwave Tech, Vol. 15, pp. 998-1005.

39. *Very High-Q Whispering-Gallery Mode Resonances Observed on Fused Silica Microspheres.* **L. Collot, V. Lefevre-Seguin. M. Brune, J.M. Raimond and S. Haroshe.** 5, 1993, Europhys. Lett., Vol. 23, pp. 327-334.
40. *Ultra-High-Q Toroid Microcavity on a Chip.* **D. K. Armani, T. J. Kippenberg, S. M. Spillane and K. J. Vahala.** 2003, Nature , Vol. 421, pp. 925-928.
41. *Integrated Optical Microcavities for Enhanced Evanescent-Wave Spectroscopy.* **E. Krioukov, D.J.W. Klunder and A. Driessen, J. Greve and C.Otto.** 17, 2002, Optics Letter, Vol. 27, pp. 1504-1506.
42. *Integrated Multiplexed Biosensors LCORR and ARROW.* **U Levya, K. Campbell and A. Groismanb, S. Mookherjea and Y. Fainman.** 2006, Applied Physics Letters, Vol. 88, p. 1111107.
43. *Nonlinear Optical Effects and Materials.* **Günter, Peter.** s.l. : Springer, 2000, pp. 3, 43, 121, 122, 131,132.
44. *Nonlinear Fiber Optics.* **Agrawal, G.** s.l. : Academic Press, 2001.
45. *Phase-Matched Excitation of Whispering-Gallery-Mode.* **J. C. Knight, G. Cheung, F. Jacques, and T. A. Birks.** 15, s.l. : Optics Letter, 1997, Vol. 22, pp. 1129-1131.

46. *Quality-Factor and Nonlinear Properties of Optical Whispering Gallery Modes.* **V.B. Braginsky, M.L. Gorodetsky and V.S. Ilchenko.** 7, s.l. : Physics Letters A, 1989, Vol. 137, pp. 393-397.
47. *Shift of Whispering-Gallery Modes in Microspheres by Protein Adsorption.* **S. Arnold, M. Khoshshima, I. Teraoka, S. Holler, F. Vollmer.** 4, 2003, Optics Letters, Vol. 28, pp. 272-274.
48. *Ultimate Q of Optical Microsphere Resonators.* **M. L. Gorodetsky, A. A. Savchenkov, and V. S. Ilchenko.** 7, 1996, Opt. Lett. , Vol. 21, pp. 453-455.
49. *High- Q Measurements of Fused-Silica Microspheres in the Near Infrared.* **D. W. Vernooy, V. S. Ilchenko, H. Mabuchi, E. W. Streed, and H. J. Kimble.** 4, 1998, Optics Letters, Vol. 23.
50. *Low-Threshold Optical Parametric Oscillations in a Whispering Gallery Mode Resonator.* **J.U. Fürst I, D.V. Strekalov, D.Elser, A. Aiello, U.L. Andersen, C. Marquardt and G. Leuchs.** 26, s.l. : Phys. Rev. Lett., 2010, Vol. 105.
51. *Optical Microsphere Resonators: Optimal Coupling to High- Q Whispering-Gallery Modes.* **V.S.Ilchenko., M.L. Gorodetsky and.** 1999, J. Opt. Soc. Am. B., Vol. 16, pp. 147-154.
52. *Analytic Theory of Coupling from Tapered Fibers and Half-Blocks into Microsphere Resonators.* **B. E. Little, J.P. Laine, and H.A. Haus.** 4, 1999, Journal of lightwave Technology, Vol. 17, pp. 704-715.

53. *Modal Coupling in Traveling-Wave Resonators*. **T. J. Kippenberg, S. M. Spillane, and K. J. Vahala**. 19, 2002, *Optics Letters*, Vol. 27, pp. 1669-1671.
54. *Fabrication and Modeling of Uniform-Waist Single-Mode Tapered Optical Fiber Sensors*. **J. Villatoro, D. Monzon-Hernandez, and E. Mejia**. 13, 2003, *Applied Optics*, Vol. 42, pp. 2278-2283.
55. *Ideality in a Fiber-Taper-Coupled Microresonator System for Application to Cavity Quantum Electrodynamics*. **S. M. Spillane, T. J. Kippenberg, O. J. Painter, and K. J. Vahala**. 4, 2003, *Physical Review Letters*, Vol. 91, pp. 043902-1-4.
56. *Observation of Critical Coupling in a Fiber Taper to Silica-Microsphere Whispering-Gallery Mode System*. **M. Cai, O. Painter and K. J. Vahala**. 2000, *Phys. Rev. Lett.*, Vol. 85, pp. 74-77.
57. *Excitation of Resonances of Microspheres on an Optical Fiber*. **A. Serpenguzel, S. Arnold, and G. Griffel**. 1994, *Opt. Lett.*, Vol. 20, pp. 654-656.
58. *Phase-Matched Excitation of Whispering-Gallery-Mode Resonances by a Finer Taper*. **J. C. Knight, G. Cheung, F. Jacques, and T. A. Birks**. 1997, *Opt. Lett.*, Vol. 22, pp. 1129-1131.
59. *Optical Microsphere Resonators: Optimal Coupling to High-Q Whispering-Gallery Modes*. **Ilchenko, M. L. Gorodetsky and V. S.** 1999, *J. Opt. Soc. Am. B.*, Vol. 16, pp. 147-154.

60. *Analytical Study of the Microdisks Resonant Modes Coupling with a Waveguide Based on the Perturbation Theory.* **A. Morand, K. Phan-Huy, Y. Desieres, and P. Banech.** 2004, *J. Lightwave Technol.*, Vol. 22, pp. 827-832.
61. *Integral Equation Analysis of Scattering by a Spherical Microparticle Coupled to a Subwavelength-Diameter Wire Waveguide.* **Uzunoglu, I. D. Chremmos and N. K.** 2, 2006, *J. Opt. Soc. Am. A*, Vol. 23.
62. *Polarization-Discriminated Spectra of a Fiber-Microsphere System.* **H. Konishi, H. Fujiwara, S. Takeuchi, and K. Sasaki.** 2006, *Appl. Phys. Lett.*, Vol. 89, p. 121107.
63. *Wavelength-Independent Coupler From Fiber to an On-Chip Cavity, Demonstrated Over an 850nm Span.* **T. Carmon I, S. Y. T. Wang, P. Ostby, and K. J. Vahala.** 2007, *Opt. Exp.*, Vol. 15, pp. 7677-7681.
64. *Second-Harmonic Rayleigh Scattering From a Sphere of Centrosymmetric Material.* **J. I. Dadap, J. Shan, K. B. Eisenthal and T. F. Heinz.** 1999, *Phys. Rev. Lett.*, Vol. 83, pp. 4045-4048.
65. *Second-Harmonic Generation in the Scattering of Light by Two-Dimensional Particles.* **C. I. Valencia, E. R. Mendez, and B. S. Mendoza.** 2003, *J. Opt. Soc. Am. B*, Vol. 20, pp. 2150-2161.
66. *Asymptotic Expansion of Morphological Resonance Frequencies in Mie Scattering.* **Schiller., S.** 12, 1993, *Applied Optics*, Vol. 32, pp. 2181-2185.

67. *Self-Assembled Monolayer Electron-Beam Resists on GaAs and SiO₂*. **M. J. Lercel, R. C. Tiberio, P. F. Chapman, H. G. Craighead, C. W. Sheen, A. N. Parikh, and D. L. Allara.** 1993, *J. Vac. Sci. Technol. B*, Vol. 11, p. 2823 .
68. *Evidence of an Electron-Induced Channel for Desorption of Ethylene from Diethylsilane-Covered Si (100)*. **J. Lozano, J. H. Craig Jr.** 2007, *Thin Solid Films* , Vol. 515, pp. 7876–7879 .
69. *Low-Energy Electron-Beam Patterning of Amine-Functionalized Self-Assembled Monolayers*. **C. K. Harnett, K. M. Satyalakshmi, H. G. Craighead.** 2000, *Appl. Phys. Lett*, Vol. 76, p. 2466.
70. *Electron Beam-Induced Damage of Alkanethiolate Self-Assembled Monolayers Adsorbed on GaAs (001): A Static SIMS Investigation* . **C. Zhou, J. C. Jones, A. Trionfi, J. W. P. Hsu, A. V. Walker.** 114, 2010, *J. Phys. Chem. C*, Vol. 12, pp. 5400–5409 .
71. *Fabrication of Surface relief Grating with Second-Order Nonlinearity Using Urethane–Urea Copolymer Films*. **Y. Che, O. Sugihara, C. Egami, H. Fujimura, Y. Kawata, N. Okamoto, M. Tsuchimori, and O. Watanabe.** 1999, *Jpn. J. Appl. Phys.*, Vol. 38, p. 6316.
72. *Strong Enhancement of Second-Harmonic Generation in All-Dielectric Resonant Waveguide Grating*. **M. Siltanen, S. Leivo, P. Voima, M. Kauranen, P. Karvinen, P. Vahimaa, M. Kuittinen.** 2007, *Appl. Phys. Lett.*, Vol. 91, p. 111109 .

73. *Second-Harmonic Generation in Resonant Waveguide Gratings Incorporating Ionic Self-Assembled Monolayer Polymer Films.* **G. Purvinis, P. S. Priambodo, M. Pomerantz, M. Zhou, T. A. Maldonado, R. Magnusson.** 2004, *Opt. Lett.* , Vol. 29, p. 1108 .

74. *Fabrication of a Distributed-Feedback Dye Laser with a Grating Structure in its Plastic Waveguide.* **Y. Oki, T. Yoshiura, Y. Chisaki, M. Maeda.** 24, 2002, *Appl. Opt.*, Vol. 41, pp. 5030-5035.

75. *Random Quasi-Phase-Matching in Bulk Polycrystalline Isotropic Nonlinear Materials.* **M. Baudrier-Raybaut, R. Haidar, Ph. Kupecek, Ph. Lemasson, and E. Rosencher.** 2004, *Nature*, Vol. 432, p. 374.

76. *Surface Second Harmonic Generation Spectroscopy Without Interference of Substrate Contributions.* **G. A. Reider, M. Huemer, and A. J. Schmidt.** 2, 1988, *Opt. Commun.*, Vol. 68, pp. 149–152.

77. *Generation and Detection of a Monolayer Grating by Laser Desorption and Second-Harmonic Generation: CO on Ni(111).* **Shen, X. D. Zhu and Y. R.** 10, 1989, *Opt. Lett.*, Vol. 14, p. 503.

78. *Second-Harmonic Diffraction From a Monolayer Grating.* **T. Suzuki, T.F. Heinz.** 21, 1989, *Opt. Lett.*, Vol. 14, pp. 1201-1203.

79. *Angular Dependence of Optical Second-Harmonic Generation from a Monolayer Grating.* **R. W. J. Hollering, Q. H. F. Vrehan, and G. Marowsky.** 5-6, 1990, *Opt. Commun.* , Vol. 78, pp. 387–392.

80. *Surface Diffusion of Co on Ni(111) Studied by Diffraction of Optical Second-harmonic Generation off a Monolayer Grating*. **X. D. Zhu, Th. Rasing, and Y. R. Shen**. 1988, Phys. Rev. Lett., Vol. 61, pp. 2883–2885.
81. *Optical Properties in Langmuir-Blodgett Films of Crystal Violet Dyes Adsorbing Cyanine Dyes*. **K. Kato, K. Shinbo, K. Obata, F. Kaneko,** 615, 2000, Synthetic Metals, pp. 111–112.
82. *Hexagonally Polled Lithium Niobate: A Two-Dimensional Nonlinear Photonic Crystal*. **N. G. R. Broderick, G. W. Ross, H. L. Offerhaus, D. J. Richardson, D. C. Hanna,** 2000, Phys. Rev. Lett., Vol. 84, p. 4345.
83. *A new Theory of Wood's Anomalies on Optical Gratings*. **A. Hessel, A. A. Oliner,** 10, 1965, Appl. Optics, Vol. 4, pp. 1275-1297.
84. *Colloquium: Light Scattering by Particle and Hole Arrays*. **García-de-Abajo, F. J.** 2007, Rev. Mod. Phys., Vol. 79, pp. 1-25.
85. *Visible Second-Harmonic Light Generated From a Self-Organized Centrosymmetric Lattice of Nanospheres*. **M. Maymó, J. Martorell, A. Molinos-Gomez and F. Lopez-Calahorra.** 2006, Opt. Exp., Vol. 14, pp. 2864-2872.
86. *Modified Triphenylmethane Dye for the Efficient Nonlinear Generation of Light in Nanostructured Material*. **X. Vidal, J. R. Herance, J. Marquet, J. L. Bourdelande and J. Martorell.** 8, 2007, Appl. Phys. Lett., Vol. 91, p. 081116 .

Table of Figures

Figure 1-1 The binding of molecules on the surface of a resonator shifts the resonant frequency. (A) A passive resonator has less resolution than (B) an active resonator. The reactive shift method can be enhanced through optical gain by improving the minimum detectable resonant shift (20), where $\Delta\nu$ is the resonance linewidth calculated from cold cavity Q factor and the gain g is the lasing mode at the WGM resonant frequency ν_0 10

Figure 2-1. Schematic representation of a WGM mode when the sphere radius is much higher than the resonant wavelength. 17

Figure 2-2. From ray optics WGM modes can be understood as a zig-zag path resulting from multiple total internal reflections. The refractive index of the sphere is n_s and the one from the surrounded media is n_0 17

Figure 2-3. Fused silica sphere microcavity image from a Scanning Electron Microscopy and the glass stem that is used to support and manipulate such microcavity. 19

Figure 2-4. a) Scheme of a tapered fiber and microsphere coupling system. Top view b) and side view c) of coupling system and experimental set-up d). 20

Figure 2-5. Schematic representation of the radial distribution intensity inside the fused silica microsphere when $p = 1, 2, 3$ and $l = m$ 23

Figure 2-6. Normalized intensity distribution in angular direction of a microsphere with $180\mu m$ in radius, where $p = 1$ and $l - |m| = 1$ (blue), 2(red) and 3(green). 24

Figure 2-7. Picture of the light scattered out from the sphere surface. Extended light distribution that seems to support the idea of multiple resonant mode coupling. 24

Figure 2-8 Doubly resonant, phase-matched micro-sphere: $(k2l, P = 2kl, p)$ a as a function of sphere radius. The choice $L = 2l$ ensures phase matching for

whispering gallery modes with $m = l$ and $M = L$. Higher radial wave number must be assumed for the second harmonic. At double resonance ($a \approx 58\mu\text{m}$) the fundamental wavelength is approximately 782nm. In order to draw this curves we assumed a Sellmeyer dispersion formula with $n(\lambda)$ coefficients given in Appendix of (25). 28

Figure 2-9. Molecular thin layer and grating at the interface of the sphere. Optimum quasi phase matching is achievable when the periods resemble the curved surface of an orange slice. 30

Figure 2-10. Coherence length ℓ_c as a function of sphere radius. Continuous line: analytical formula; circles: numerically computed values from an 8-order asymptotic expansion relating mode frequency and mode orbital and radial numbers (66). The fundamental wavelength is $\lambda = 800 \text{ nm}$. Only modes with $m = l, M = L,$ and $p = P = 1$ are considered..... 31

Figure 3-1. Schematic view of the experimental set-up used for measuring the diffracted second harmonic light (TS stands for translation stage). Inset (left): writing of a periodic $\chi^{(2)}$ pattern onto the molecular film by SEM. The nonlinear activity of the molecule is quenched by e-beam irradiation. 37

Figure 3-2 Second harmonic (SH) generation scans across different film regions (measured in reflection) as indicated in the schematic view of the experimental set-up: (a) pristine film [dotted black line]; (b) film region with two gratings of

same period but different width α of the exposed stripes[dotted blue line]; and
 (c), film region with one grating of same previous period ratio and upon totally
 irradiated area ratio[dotted red line]. 39

Figure 3-3. Second harmonic diffraction patterns from gratings of different period
 ((a), $\delta = 40, 20, 10 \mu\text{m}$; (b) $\delta = 4 \mu\text{m}$), with the fundamental beam impinging at
 45° . The angular spacing between the diffraction peaks matches the
 expectations for second harmonic diffraction at a wavelength of 400 nm for the
 various periods used for the lithography. The intensity of the specular ($m = 0$)
 order is saturated in the detector. 41

Figure 4-1 . Crystal Violet Molecule. 45

Figure 4-2. The number of CV molecules per unit surface times the cross-section of
 CV as a function of the molar concentration of the solution used for a coating
 layer. Inset: absorbance spectra for three monolayers representative of the
 eight monolayers prepared. 47

Figure 4-3. Equation (2-16) as a function of the radius of the sphere and wavenumber
 for the fundamental wave in vacuum. The arc length is fixed to $8.8 \mu\text{m}$ at the
 equator. 48

Figure 4-4. SEM image of the microsphere used in the experiment. The periodical
 pattern drawn on the sphere is superimposed on the SEM image of the sphere

at the same scale. The diameter of the sphere was $359\mu m$. Inset: Change in z direction perpendicular to the e-beam. 49

Figure 4-5. Pattern preparation at the electron beam lithography with a periodic pattern of domains of width ℓc as given in equation (2-16). 50

Figure 4-6. Schematic view of the experimental set-up used for measuring the SH light generated by the nonlinear grating at the surface of the microsphere. The fiber loop is used only in the experiments where the fundamental pulse is stretched to uniformly cover the entire perimeter of the sphere. The inset shows the polar and radial distribution of the WGM when the pulse is coupled into the microsphere (bright spot on the right). The picture was taken for a sphere doped with Erbium atoms to facilitate the visibility of the WGM. The other two spots on the left correspond to images or parasitic reflections formed by the sphere of the residual light uncoupled from the taper to the sphere. 52

Figure 4-7. Second harmonic generation as a function of half the wavelength of the fundamental wave (red dots) when the coating solution was $2.5 \times 10^{-4} M$. Experimental domain width minus the calculated coherence length at the equator as a function of half the wavelength of the fundamental wave in a logarithmic scale (blue solid line). The lines are only a guide for the eye. 54

Figure 4-8. SHG as a function of half the wavelength of the fundamental wave when the pump wavelength is centered at 900 nm [$2.5 \times 10^{-4} M$]. The red dotted

lines indicate the wavelength for the quasi-phase matching condition calculated using an analytical approximate expression (2-16) minus the experimental domain width. The lines are only a guide for the eye. 55

Figure 4-9. SH intensity as a function of time, using a sphere with $Q = 1.83 \times 10^7$ (red solid line) and a sphere with $Q = 3.72 \times 10^6$ (blue solid line). Both spheres were coated with a $5 \times 10^{-7} M$ solution of CV and periodically patterned to achieve the phase-matching condition. All the parameters of the experimental setup, coupling taper, input intensity and so on were kept equal. The difference in Q factor must be attributed mostly to a difference in the eccentricity, whereas the difference in radius between the two spheres was only 16% one in the vertical scale corresponds to an intensity current of $96 \mu A$ 59

Figure 4-10. Second harmonic signal in arbitrary units for four different surface concentration of nonlinear molecules when a grating was written (blue bars) and when no grating was written (red bars). In the horizontal axis we indicate the concentration of the original solution used to prepare the monolayers. 64

Figure 4-11. Natural logarithm of the measured SH intensity decrease produced when subsequent 1 sec UV flashes (horizontal axis) were shone on the sphere to photodegrade the CV. The background noise is subtracted from the measured intensity and then such difference divided by the reference input intensity to ensure a unitless logarithm argument and proportionality to the molecular surface density. Two different spheres were coated with a $1.55 \times 10^{-9} M$

solution of CV (green dots) and with a $1 \times 10^{-7} M$ solution of CV (red dots). The numbers by the green dots should not be taken literally and are only indicative of the molecules that participate in the SHG prior to the shining of each UV flash. The solid lines indicate a linear adjustment to the portion of data that shows a decrease while the dotted lines indicate a linear adjustment to the almost flat portion of the data. 68